Trakya Üniversitesi
Mühendislik Bilimleri Dergisi

Cilt: 16 Sayı: 2 Aralık 2015

TRAKYA UNIVERSITY JOURNAL OF ENGINEERING SCIENCES

Volume: 16 Number: 2 December 2015

Trakya Univ J Eng Sci

http://dergipark.ulakbim.gov.tr/tujes
tujes@trakya.edu.tr

ISSN 2147-0308

Trakya Üniversitesi
Mühendislik Bilimleri Dergisi

Cilt: 16 **Sayı: 2** **Aralık** **2015**

Trakya University
Journal of Engineering Sciences

Volume: 16 **Number: 2** **December** **2015**

Trakya Univ J Eng Sci

http://dergipark.ulakbim.gov.tr/tujes
tujes@trakya.edu.tr

ISSN 2147-0308

Dergi Sahibi / Owner
Trakya Üniversitesi Rektörlüğü, Fen Bilimleri Enstitüsü Adına
On behalf of Trakya University Rectorship, Graduate School of Natural and Applied Sciences
Prof. Dr. Mustafa ÖZCAN

Baş Editör / Editor-in-Chief
Doç. Dr. Hacı Ali GÜLEÇ

Yardımcı Editörler / Associate Editors
Doç. Dr. Cem S. ÇETİNARSLAN
Yrd. Doç. Dr. Esma MIHLAYANLAR
Yrd. Doç. Dr. Altan MESUT
Yrd. Doç. Dr. A. Can ZÜLFİKAR

Dizgi / Design
Yrd. Doç. Dr. Altan MESUT, altanmesut@trakya.edu.tr
Taylan ŞAHİNBAŞ, taylansahinbas@hotmail.com

İletişim Bilgisi / Contact Information
Address : Trakya Üniversitesi, Enstitüler Binası, Fen Bilimleri Enstitüsü,
Balkan Yerleşkesi, 22030, Edirne / TÜRKİYE
Web site : http://dergipark.ulakbim.gov.tr/tujes
E-mail : tujes@trakya.edu.tr
Tel : +90 284 2358230
Fax : +90 284 2358237

Baskı / Publisher
Trakya Üniversitesi Matbaa Tesisleri
Trakya University Publishing Centre

ISSN 2147-0308

Editör Kurulu / Editorial Board

ISSN 2147-0308

İÇİNDEKİLER / CONTENTS

A Constitutive Material Model for Restrained Reinforced Concrete Columns in Case of Fire – Part I
Ataman HAKSEVER **43-53**

Numerical Study of Pressure Drop in the Horizontal Spirally Coiled Tubes
Omid SEYEDASHRAF **55-60**

The Effects of Geotextile Layers on Bearing Capacity of Gravel-Silt Mixtures
Keramat SADEGHI AZAR, Rouzbeh DABIRI **61-69**

ISSN 2147-0308

http://dergipark.ulakbim.gov.tr/tujes
Trakya University Journal of Engineering Sciences, 16(2): 43-53, 2015
ISSN 2147–0308
Araştırma Makalesi / Research Article

A CONSTITUTIVE MATERIAL MODEL FOR RESTRAINED REINFORCED CONCRETE COLUMNS IN CASE OF FIRE PART I

Ataman HAKSEVER

Department of Civil Engineering, Namık Kemal University, Tekirdağ, TURKEY
ahaksever1@gmail.com

Abstract: In the eighties increased basic research was carried out in **SFB** (**S**onder**F**orschungs**B**ereich: a special fire research activity for structural elements in Braunschweig Technical University, 1971-1986) in order to clarify the discrepancies between calculation and measurement of restrained compression elements in case of fire. The work was particularly focused on the description of a universal material model for the concrete under elevated temperatures that could be applied successfully to estimate the relaxation response of restrained compression columns in fire. In the literature, various material models for structural concrete can be found. In many cases, however, the verification of such models lacks for the case of fire, especially when a mechanical restraining or caused by the entire structural interaction of the carrying system is present.

Keywords: Fire action, Structural fire safety, material model for the concrete, restrained compression elements

UN MODELE DE MATERIAU CONSTITUTIF POUR COLONNES EN BETON ARME RESTREINT EN CAS D'INCENDIE PART I

Résumé: Dans les années quatre-vingt a augmenté la recherche fondamentale a été réalisée en **SFB** (Une activité spéciale de recherche sur le feu pour les éléments structurels de l'Université Technique de Braunschweig, 1971 à 1986) afin de clarifier les écarts entre calcul et mesure des éléments de compression restreint en cas d'incendie. Le travail a été particulièrement axée sur la description d'un modèle de matériau universel pour le béton sous des températures élevées qui pourraient être appliquée avec succès pour estimer la réponse de relaxation de colonnes de compression restreint dans le feu. Dans la littérature, différents modèles de matériaux pour le béton structurel peuvent être trouvés. Dans de nombreux cas, cependant, la vérification de ces modèles ne dispose pas dans le cas d'incendie, surtout quand une restreint mécanique ou causée par l'ensemble de l'interaction structurelle du système est présent.

Mots clés: Action incendie, Structurel sécurité en cas d' incendie, modèle de matériau béton, relaxation de colonnes

INTRODUCTION

In the eighties increased basic research was carried out in SFB in order to clarify the discrepancies between calculation and measurement of restrained compression elements in case of fire. The work was particularly focused on the description of an universal material model for the concrete by a comprehensive mathematical formulation of the rheological phenomena's under elevated temperatures that could be applied successfully to estimate the relaxation response of restrained compression columns in fire.

It was well known that the use of such material model would require an immense effort in calculator. The computational studies have shown, however, that such effort is worthwhile, because only by a realistic material model fire behavior of restrained structural elements can be estimated satisfactorily for fire case **(Bazant, Z. P., 1982)**. It should be emphasized here that a material model can gain confidence only if it has been tested for various structural elements and fire conditions.

In particular, the model must apply for the assessment of the fire behavior of structural elements in practical sizes. In the literature, various material models for structural concrete elements can be found. In many cases, however, the verification of such models lacks for the case of fire, especially when a mechanical restraining or caused by the entire structural interaction is present.

Literature review (1973-2014)

Upmeyer, J., and Schaumann, P. show in their contribution studies to fire resistance of reinforced concrete columns, based on a structural analysis with an advanced calculation model. The analysis covers simply supported columns as well as cantilever columns with buckling length in case of fire up to 20.0 m. Finally safety considerations for reinforced concrete columns will be performed, which show, that existing concrete columns, which are designed in conformity with the minimum dimensions of German Standards (table 31 in DIN 4102-4), are stable in case of fire, if they are planned and built in compliance to acknowledged rules of technology.

Cyllok, M., and Achenbach, **M**. give information to their labor tests. The application of nonlinear zone method is explained. The statistical

evaluation leads to governing key data, which proof adequate safety according to DIN 4102-2. Research work shows that the nonlinear zone method (simplified calculation method) can be used for design of reinforced concrete columns exposed to fire. The decisive action effects of a fire exposure on the structural behavior are considered by this method and have been proofed by a comparison of ultimate loads and deformation curves computed by using nonlinear zone method as well as using advanced method. In addition, this article statistically evaluates how safe – according to **DIN 4102-2** – published full scale tests that can be modeled by using nonlinear zone method. Information to mentioned tests is shown.

Frank Fingerloos, F and Richter, E. explain the background of the structural fire design of reinforced concrete columns with a modified new fire design-table in the German standard **DIN 4102**. The limit condition of according to this table results show often with a maximum 6 m length for rectangular columns and 5 m length for circular columns very conservative reinforcements and dimensions. For these cases it is proposed an extension of the fire design- table. An example completes the paper.

Sven Huismann. S. And , Manfred Korzen, M, and Andreas Rogge, A. discuss in their paper following a critical analysis of the material parameters of normal strength (NSC) and high strength concrete (HSC) presented in **Eurocode 2** the thermo-mechanical material parameters of one representative HSC. Using these parameters and based on an appropriate material model the behavior of HSC columns was simulated. It was found that the strength as a characteristic parameter of the material model has to be identified on the basis of transient creep tests and not of stationary tests, respectively as realized usually for NSC

Quast. U. states that the consistent distinction between stress-dependent and thermal strains is essential for nonlinear calculation fire induced cross-sections. Even for non-linear cross section calculations with prestressed reinforcement, taking into account the effects of creep and shrinkage or other issues, the concept of stress-dependent strain is appropriate. It results in a total uniform approach for the formulation of the strain state.

Lange, D., and Sjöström, J. describe in their paper the effect of thermal exposure varying in both the horizontal and vertical axes to columns by means of including this thermal boundary in a solution of classical Euler beam theory. The resulting solution allows for a variation in the stiffness of the rotational restraint at both ends of the column and a non-uniform temperature exposure through the column's section and along its height.

Xu, Y., Wu, B. obtain in their experimental results that: When the axial load ratio is 0.55, the fire resistances of the columns with L-, T-, and +-shaped cross-sections subjected to fire on all sides were 60–73% that of the column with the square cross-section under design loads. A computer program RCSSCF was developed to calculate temperature, deformation, and fire resistance of the loaded columns with different shaped cross-sections. It is stated that the results of the numerical simulation were compared with those of the full-scale fire resistance tests.

Franssen, J.-M. presents the basic principles of the arc-length technique, first for the way it is applied traditionally at room temperature, then for the way it can be applied to extend a numerical simulation beyond the moment of local failures in case of fire. The technique is then applied to the case of restrained columns and it is shown how it is possible to obtain a safe estimate of the critical temperature of the column leading to the failure of the structure, even if the degree of restraint applied to the column is unknown.

Nguyen, T.-T., Tan, K. H. give a simplified analytical model to directly determine these so-called thermal-induced restraint forces. The model bases on the concepts of equivalent distributed temperature as well as eccentricity- and temperature-dependent reduction factor of axial stiffness. The model is validated by fire tests conducted at Nanyang Technological University on twelve restrained concrete column specimens subjected to uniaxial and biaxial bending. Relatively good agreement between the analytical and the experimental results of restraint force development is obtained.

Neves, N., Valente, J.C., Rodrigues, J. P. C., make a proposal which uses the results of a series of tests and calculations, with the aim of being applied as a simple method to correct the value of the critical temperature of steel columns free to elongate, in order to take into account the restraint effect of the structure to which they belong in a practical situation.

Consequences of the Material Modeling for Concrete

In this paper, an approach is shown to take into account the material behavior of normal concrete as realistically as possible in restraining condition of structural elements. Concrete is one of a group of materials showing time dependent deformation under acting load. The portion of the total deformation occurring, which remains after deduction of the elastic ε_{el} and thermal expansion ε_{th} as well as independent shrinkage ε_s deformations of the load is commonly referred to as a creep deformation ε_{cr}.

The creep of concrete under elevated temperatures has been studied in a variety of researchers (**Waubke, N. Y.,** 1973**., Schneider, U.,** 1973**. and**

Anderberg, Y., 1976). In the context of this article, however, focus is laid only on the work of the SFB and Swedish researchers who have carried out intensified work as special material research to clarify the high-temperature creep of concrete. In the Lund Institute of Technology material model presented by Anderberg describes the total deformation of the concrete as given Eq. 1:

$$\varepsilon_{tot} = \varepsilon(\sigma(t), T(t), \tilde{\sigma}) \quad (1)$$

In Eq. 1 the stress history of the concrete $\tilde{\sigma}$ is represented under high temperature effect. The total deformation ε_{tot} consists of several components; the individual variables however are associated with a certain experimental procedure. The Eq. 1 is given in explicit form as follows:

$$\varepsilon_{tot} = \varepsilon_{th} + \varepsilon_{\sigma}(\tilde{\sigma}, \sigma, T) + \varepsilon_{scr}(\sigma, T, t) + \varepsilon_{tcr}(\sigma, T) \quad (2)$$

In this equation ε_{th} thermal expansion, ε_{σ} spontaneous stress dependent compression, ε_{scr} stationary creep and ε_{tcr} transient creep are the strains under a certain compression stress. The determination of the deformation components are discussed in detail in **(Anderberg, Y.,** 1976**).** Anderberg formulates the transition creep as a spontaneous reaction to the effect of temperature and converts it as a time dependent deformation which is assumed linearly related to the present stress. The Eq. 2 results in by this way into Eq. 3:

$$\varepsilon_{tot} - \varepsilon_{th}(T) - \varepsilon_{tcr}(\sigma, T) = \varepsilon_{\sigma} + \varepsilon_{scr} \quad (3)$$

For the accurate determination of the right side of this equation, a special importance is attached, because the stress generating deformation components in the calculation must be determined successively with certain time intervals. Research in SFB of this nature has already been completed **(Waubke, N. V.,** 1973**., Schneider., U.,** 1973**).** As an illustration of the phenomenon that with a load of concrete, the deformations of the building material increase over time, a relationship implicit form is required as given in Eq. 4:

$$F = (\varepsilon, \sigma, \tilde{\sigma}, t, T) = 0 \quad (4)$$

In Eq. 4 it is assumed that the differential and integral operators of the functions ε, σ, and t are known. **(Schneider, U.,** 1973**)** therefore the total deformation in Eq. 4 attempted to describe in accordance with the usual method at room temperature. Then a creep relationship as easy as possible was developed by determination of *φ-values*. According to Eq. 5 it is possible to describe the total deformation of concrete at a constant compression stress as follows:

$$\varepsilon_{tot=}\, \varepsilon_{th} - \big(1 + \varphi(T, t)\big) \frac{\sigma}{E(T)} \quad (5)$$

The Eq. 5 can also be expressed in another form to determine the stress condition (See Figure 6 for the function of modulus of elasticity):

$$\sigma = (\varepsilon_{tot} - \varepsilon_{th)}.E(T) - \varphi(T, t).\sigma \quad (6)$$

By means of the determination of *φ(T,t)* the present problem would be solved. The difference *($\varepsilon_{tot} - \varepsilon_{th}$)* in Eq. 5 gives the desired deformation term, which can be split into an elastic and inelastic strain components. The latter component corresponds to the time dependent deformation parts which occur under compression stress and unsteady ~~t~~emperature effects. It is defined by **(Schneider, U.,** 1985**)** as it reads in Eq. 7:

$$(\frac{\partial \varepsilon}{\partial t})_{\sigma} = \sigma(\frac{\partial J(\sigma,t)}{\partial t})_{\sigma} \quad (7)$$

In Eq. 7 *J(σ,t)* corresponds to the creep function. It was determined by means of creep tests at unsteady temperatures, for a given constant compression stress *(hot creep tests).* The total deformation can thus be determined according to Eq. 8 for a given compression stress and for a given initial deformation$\varepsilon_{0:}$

$$\varepsilon_{tot=}\, \varepsilon_0 + \frac{\sigma}{E(T)} + \sigma.J(\sigma, T) \quad (8)$$

From here it results in an equation for determining *J(σ,T)*:

$$J(\sigma, T) = \frac{1}{E(T)}.\varphi(\sigma, T) \quad (9)$$

In case of fire, however, temperature and stress changes occur in a concrete element. It is therefore not possible to apply Eq. 8 for creep problems in this form, because the determination of the total deformation results in integral equations.

Problem Definition

Reinforced concrete columns are generally in interaction with their surroundings if they are monolithic constructed with the structural system **(Kordina, K.,** 1979**., Anderberg, Y.,** 1976**).** Thereafter, against the free thermal expansion of a fire exposed reinforced concrete column in a building an elastic restraining takes action. In this case variable axial restraining forces can develop bound to the grade of elastic restraining during the fire.

The restraining tests carried out with reinforced concrete columns in the special furnace of SFB have proven that between the prediction and the measured axial restraining forces during the fire significant deviations occurred. Therefore to clarify this discrepancy an intensive research was accomplished. Research focused in particular on the realistic description of the material behavior of concrete in case of fire **(Kordina, etal.,** 41. Jahrg**).** In addition, other new tests were carried out with different cross-sectional sizes and column slenderness. In fact, such a constitutive material law was developed through a close collaboration of scientists from different subprojects ***A and B3*** of the ***SFB.***

AN ANALYTICAL MATERIAL MODEL FOR HIGH-TEMPERATURE

Deformation Components of Concrete at High Temperatures

The total deformation of concrete under unsteady temperature exposure has at least 5 individual deformation components. The total deformation ε_{tot} can be described as given in Eq. 10:

$$\varepsilon_{tot} = \varepsilon_{th} + \varepsilon_s + \varepsilon_{el} + \varepsilon_{pl} + \varepsilon_{cr} \quad (10)$$

It can be assumed that the shrinkage component was included in the thermal expansion from Eq. 10 results in Eq. 11:

$$\varepsilon_{tot} - \varepsilon_{th} = \varepsilon_{el} + \varepsilon_{pl} + \varepsilon_{cr} \quad (11)$$

Eq. 11 therefore displays the sum of the stress generating deformation components minus the thermal expansion from the total deformation.

Modeling of the Stress History

In this section it will be shown mathematically that the inclusion of a stress history for concrete is essential. Multiplication the both sides of Eq. 11 by *E(t)* gives Eq. 12 and with definition of new deformation components, the following equations can be written:

$$E(t).(\varepsilon_{tot} - \varepsilon_{th}) = E(t).(\varepsilon_{el} + \varepsilon_{pl} + \varepsilon_{cr}) \quad (12)$$

$$\varepsilon_1 = \varepsilon_{tot} - \varepsilon_{th} \quad (13)$$

$$\varepsilon_2 = \varepsilon_{el} + \varepsilon_{pl} + \varepsilon_{cr} \quad (14)$$

and the total differential Eq. 12 results in Eq. 15:

$$\frac{\partial}{\partial t}(E(t).\varepsilon_1).dt = \frac{\partial}{\partial t}(E(t).\varepsilon_2).dt \quad (15)$$

By introducing the functions *U* and *V*

$$V(t) = \varepsilon_1 \frac{\partial}{\partial t}E(t) + E(t)\frac{\partial}{\partial t}\varepsilon_1 \quad (16)$$

$$U(t) = \varepsilon_2 \frac{\partial}{\partial t}E(t) + E(t)\frac{\partial}{\delta t}\varepsilon_2 \quad (17)$$

The Eq. 17 contains the following strain rates:

For the first expression in Eq. 17

$$\varepsilon_2 \frac{\partial}{\partial t}E(t) = \varepsilon_{el}\frac{\partial}{\partial t}E(t) + \left(\varepsilon_{cr} + \varepsilon_{pl}\right)\frac{\partial}{\partial t}E(t) \quad (18)$$

Following the usual procedure results in for the second term for room temperature:

$$E(t)\frac{\partial}{\partial t}\varepsilon_2 = E(t)\frac{\partial}{\partial t}\left[\frac{\sigma\varphi}{E(t)} + \varepsilon_{pl}\right] + E(t)\frac{\partial}{\partial t}\varepsilon_{pl} \quad (19)$$

After conversion of Eq. 19

$$E(t)\frac{\partial}{\partial t}\epsilon_2 = E(t)\frac{\partial}{\partial t}\varepsilon_{el} + E(t)\frac{\partial}{\partial t}\left[\sigma\frac{\varphi}{E(t)}\right] + E(t)\frac{\partial}{\partial t}\varepsilon_{pl} \quad (20)$$

The total stress variation results in consequently from the summation of Eqs. 18 and 20:

$$U(t) = E(t)\frac{\partial}{\partial t}\varepsilon_{el} + \varepsilon_{el}\frac{\partial}{\partial t}E(t) + E(t)\frac{\partial}{\partial t}\left[\sigma\frac{\varphi}{E(t)}\right] + \varepsilon_{cr}\frac{\partial}{\partial t}E(t) + \varepsilon_{pl}\frac{\partial}{\partial t}E(t) + E(t)\frac{\partial}{\partial t}\varepsilon_{pl} \quad (21)$$

In case of leaving out of consideration the time independent deformation components in Eq. 20 the function *U(t)* gets the form as given in Eq. 22:

$$U(t) = \dot{\sigma} + E(t)\frac{\partial}{\partial t}\left(\sigma\frac{\varphi}{E(t)}\right) + (\sigma.\varphi)\frac{\dot{E}(t)}{E(t)} + \varepsilon_{pl}.\dot{E}(t) \quad (22)$$

and in Eq. 22 a new function defined as Z(t):

$$Z(t) = E(t)\frac{\partial}{\partial t}\left(\sigma\frac{\varphi}{E(t)}\right) \quad (23)$$

$$Z(T) = E(t)\left[\frac{\varphi}{E(t)}.\frac{\partial\sigma}{\partial t} + \sigma\frac{\partial}{\partial t}\left(\frac{\varphi}{E(t)}\right)\right] \quad (24)$$

and *U(t)* takes the form:

$$U(t) = \dot{\sigma} + \sigma.E(t)\frac{\partial}{\partial t}\left(\frac{\varphi}{E}\right) + \varphi.\frac{\partial\sigma}{\partial t} + (\sigma.\varphi)\frac{\dot{E}(t)}{E(t)} + \varepsilon_{pl}.\dot{E}(t) \quad (25)$$

After further conversion finally Eq. 26 can be obtained:

$$U(t) = (1+\varphi).\dot{\sigma} + \sigma\left[E(t).\frac{\partial}{\partial t}\left(\frac{\varphi}{E}\right) + \varphi.\frac{\dot{E}(t)}{E(t)}\right] + \varepsilon_{pl}.\dot{E}(t) \quad (26)$$

Now new function *Q(t)* can be defined using Eq. 27:

$$Q(t) = \frac{(U(t)-\varepsilon_{pl}.\dot{E}(t)}{(1+\varphi)} \quad (27)$$

then the decisive equation for describing the stress history is obtained:

$$Q(t) = \dot{\sigma} + \sigma\frac{1}{1+\varphi}\left[E(t)\frac{\partial}{\partial t}\left(\frac{\varphi}{E}\right) + \varphi.\frac{\dot{E}(t)}{E(t)}\right] \quad (28)$$

The Eq. 28 can be transformed into a simpler form as Eq. 29:

$$Q(t) = \dot{\sigma} + R(t) \quad (29)$$

It is clear from Eq. 29 that the determination of the actual compressive stress on a concrete element, the knowledge about the stress history is essential. By using Eq. 16 and Eq. 29 local compressive stresses can be determined:

$$V(t) = U(t) \quad (30)$$

The calculation process is described in detail in the following section.

Successive Calculation of the Compressive Stresses

In order to determine the current compression stress in a concrete element, it is necessary to integrate the Eq. 29. First partial derivatives E and φ of Eq. 28 show the significance of the functional dependence of these parameters. These arithmetic operations are given below in Eq. 32 through Eq. 35, wherein the relation with Eq. 31 is introduced.

$$\chi = \frac{\varphi(\sigma,T)}{E(\sigma,T)} \text{ s. also Fig. 28} \quad (31)$$

$$\frac{\partial E}{\partial t} = \frac{\partial E}{\partial \sigma}.\frac{\partial \sigma}{\partial t} + \frac{\partial \sigma}{\partial T}.\frac{\partial T}{\partial t} \text{ s. also Fig. 6} \quad (32)$$

$$\frac{\partial \varphi}{\partial t} = \frac{\partial \varphi}{\partial \sigma}.\frac{\partial \sigma}{\partial t} + \frac{\partial \varphi}{\delta T}.\frac{\partial T}{\partial t} \text{ s. also Fig. 7} \quad (33)$$

$$\frac{\partial \chi}{\partial \sigma} = \frac{1}{E}.\frac{\partial \varphi}{\partial \sigma} - \frac{\varphi}{E^2}.\frac{\partial E}{\partial \sigma} \quad (34)$$

$$\frac{\partial \chi}{\partial T} = \frac{1}{E}.\frac{\partial \varphi}{\partial T} - \frac{\varphi}{E^2}.\frac{\partial E}{\partial t} \quad (35)$$

It is thus clear that, the Eq. 29 to Eq. 35 the effects of temperature rate $\dot{T}$ and its following appearances must be considered in the development of material law.

The general solution of Eq. 29 is known **(Bronstein-Semendjajew,** 1973**)** and can be written with Eq. 36:

$$\sigma = e^{-\int_0^t R(t)dt}.\left[\int Q(t).e^{\int R(t)dt}\, dt + C\right] \quad (36)$$

The evaluation of Eq. 36, however, in this form is hardly possible because the σ in Eq. 36 is implied.

Considered boundary conditions as

$$t = t_0 \text{ and } \sigma = \sigma(t_0) \quad \text{bzw} \quad \sigma = \sigma_0 \quad (37)$$

The compressive stress of concrete at a given time is therefore determined incrementally. The stress variation during a time step Δt can therefore be determined by total differentials of Eq. 36. From Eq. 36 the stress determination follows with finite extents stepwise with the help of Eq. 38.

$$\sigma_t = \sigma_{t-1}.e^{-R(t).\Delta t} + s(t) \quad (38)$$

in which

$$s(t) = e^{-R(t).\Delta t}\{Q(t).e^{R(t).\Delta t}.\Delta t\} \quad (39)$$

and determination of the stress variation is carried out according to Eq. 40

$$\Delta\sigma_t = \sigma_{t-1}\left(e^{-R(t).\Delta t} - 1\right) + s(t) \quad (40)$$

The determination of the function value of *R(t)* in the above expression takes place in accordance with the agreements made in Eq. 29. In this regard, the equations 32 to 35 must be calculated successively.

According to some conversion operations *R(t)* results in Eq. 41 for a certain time duration

$$R(t) = \frac{1}{1+\varphi_t(T,\sigma)}\left\{\varepsilon(t).\left[\frac{\Delta\chi}{\Delta\sigma}.\dot{\sigma} + \frac{\Delta\chi}{\Delta T}.\dot{T}\right] + \left(\frac{\varphi}{E}.\dot{E}\right)\right\} \quad (41)$$

In order to determine the function value *Q(t)* in the stress expression Eq. 39, functional equation *V(t) = Q(t)* must be solved in Eq. 27. Infinite differences form *V(t)* can be written as in Eq. 42

$$V(t) = \varepsilon_1.\frac{\Delta E}{\Delta\sigma}.\dot{\sigma} + \varepsilon_1.\frac{\Delta E}{\Delta T}.\dot{T} + E(t).\dot{\varepsilon}_1 \quad (42)$$

From the equations 41 and 42 it is clear that at any given time of the fire duration besides the temperature rate $\dot{T}$, the stress rate $\dot{\sigma}$ has to be determined in order to calculate the actual stress in an element of concrete. Whereas the $\dot{T}$ can be determined without difficulty, however determination of $\dot{\sigma}$ is only possible iteratively.

The determination of the plastic deformations **(Schneider,** 1986**)** succeeds according to Eq. 43 for certain fire duration.

$$\varepsilon_{pl} = \frac{1}{3}.\left(\frac{\sigma}{E}\right)_t.\left(\frac{\sigma}{f_c}\right)^5 \quad (43)$$

The concrete strength f_c, E-modulus and creep function φ will be taken into account in the following functional relations:

$$f_c = f_c\left(T,\dot{T}\right) \quad (44)$$

$$E = E\left(T,\dot{T},\sigma\right) \quad (45)$$

$$\bar{\varphi} = \bar{\varphi}\,(\sigma,T,w) \quad (46)$$

In Eq. 46 *w* indicates the humidity of concrete in weight-percent.

The conducted extensive computational studies have shown that a modified new creep function $\bar{\varphi}$ must be represented as a product of two functions. This was therefore necessary because, in order to calculate the development of deformations of a concrete structural element at high temperatures, the long-time creep effects on one hand, and the influence of the cross-sectional shape on the other hand should be taken into account. The calculations results in

$$\bar{\varphi} = \psi(t,r_s,r_z).\varphi(\sigma,T,w) \quad (47)$$

whereby ψ is described **(Schneider,** 1986**)** with an empirical Eq. 48

$$\psi = \left(\frac{r_s}{r_z}\right)^{0.5} + 5.10^{-3}.t \quad (48)$$

In this equation, the time *"t"* is in minute and *"r_s"* applies for the hydraulic radius of the large specimen, and *"r_z"* for the hydraulic radius of the small specimen, which have been used in the material science. Here *"r_z"* is set 8.0 cm **(Bazant,** 1982**)**. Experimental investigations have also shown that the thermal expansion of the concrete is also affected by the dimensions of the test specimen. In order to consider this concern in calculations, only 85% of the thermal expansion of the concrete for

big structural elements at high temperatures is taken into account

Approach to the Tensile Strength of Concrete

The tensile strength of the concrete is taken into account in the calculations up to 150 °C **(Waubke, N. V.,** 1973**).** Maximum permissible tensile strength is set 1/10 the size of the current temperature depending on the compressive strength. In the determination of the tensile strength, time influences will not be considered. The cracked concrete elements subsequently are used for the compressive stresses in case of compression.

THE STRESS-STRAIN PARAMETERS INFLUENCING THE DEFORMATION DEVELOPMENT AT HIGH TEMPERATURES

Thermal Expansion

Influence of the heating rate

In Figure 1, the measured thermal expansion of the specimen is shown via the furnace temperatures. In order to determine the influence of heating rates, two distinctly different temperature increases were simulated in the furnace. In Figure 1 it can be seen that at low heating rate due to almost homogeneous temperature distribution in the cross-section significantly higher thermal expansion occurs along the longitudinal axis of the samples. From this it can be concluded that at lower heating modes higher restraint forces shall be activated in the structural concrete elements than the ISO834 fire is present.

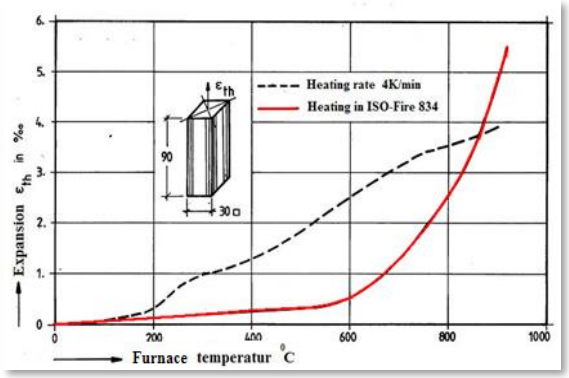

Figure 1: Influence of heating rates on the expansion of small concrete specimens obtained in SFB-Tests

Influence of the size of the specimens

In Figure 2, the thermal expansion of two different sized specimens is shown via the oven temperatures at a heating rate 4K/min. It is being clear that the specimens show at the same furnace temperature greatly differentiated thermal expansions. The higher thermal expansions occur at smaller specimens. The control calculations have shown, however, those other influences of the rheological side should be effective, such as the moisture transport and structural distortions in the element and the inner stress conditions.

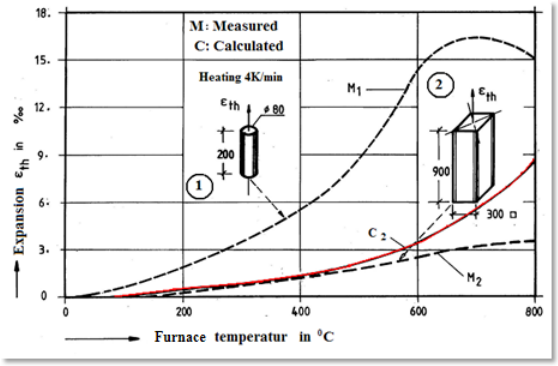

Figure 2: Measured and calculated thermal expansion of concrete specimens in different sizes

In Figure 3 however thermal expansions of the two different sized macro specimens are illustrated over time. The heating of the samples are carried out according to the ISO834-Fire Curve. The small sample body has a section along the column axis of the second macro specimen. The illustration of the test results shows also in this case, a significant difference in the development of thermal expansion of the specimens. It is clear that the small test specimens have, also in this case a higher thermal expansion

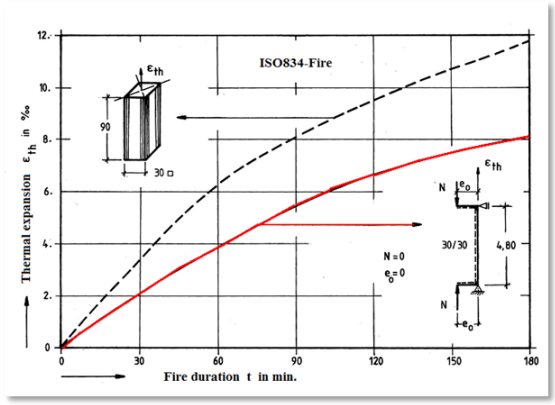

Figure 3: Thermal expansions of the two different sized macro specimens under the same heating conditions.

The results shown in figures 1 to 3 thus make the influence of specimen geometry on the development of pure thermal expansions of the specimens significant.

In order to take into account these influences and other imponderables in the numerical treatment of the material behavior, thermal expansion obtained from the small specimens was reduced by 15% (see conclusions in subsection *"Successive calculation of the compressive stresses"* and Figures 1, 2 and 3).

Influence of temperature history

The rheological tests carried out have shown that the thermal expansion of the concrete specimens indicates an irreversible behavior during the heating and cooling cycles **(Schneider, U., 1985)**. In particular, during the cooling phase of the concrete a permanent expansion remains.

In Figure 4, this behavior is illustrated via temperature. From the picture it is clear that the amount of the remaining strains depends on the maximum temperatures at a point of cross section in concrete attained. At higher temperatures also correspondingly high remaining expansion results in. They are up to a temperature of 400 °C negligible, so that in this temperature range, a quasi-reversible behavior of the thermal expansion of the concrete can be accepted. It is thus clear that the numerical treatment of concrete structures in fire, particularly in natural fires the consideration of the temperature history is inevitable.

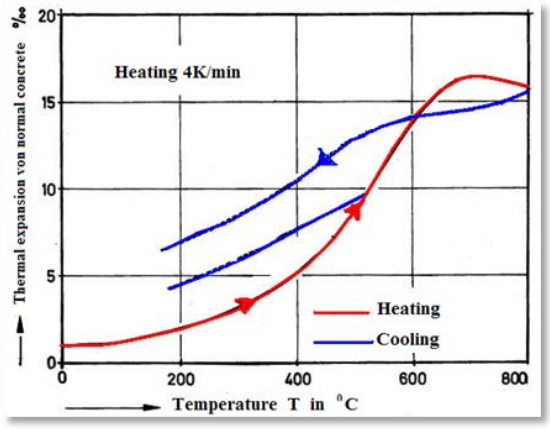

Figure 4: Effect of warming and cooling processes on the thermal expansion of the normal concrete

Influence of Heating Rate on the Concrete Strength

Loss of strength of concrete in the range of 70 to 200 °C is caused mainly by the evaporation of the physically bound water in concrete (**Ehm, C., 1985**). This process of evaporation of physically bound water is complete at about 200 °C. Until reaching this temperature limit a large pressure slope is formed in the concrete, but that is also dependent on the porosity. When a steam pressure is built up in the concrete, the high internal pore pressure and the external mechanical restrains may cause to premature failure of the specimen.

In Figure 5, this phenomenon is illustrated depending heating rate of the concrete. The figure shows the effect of temperature on the related loss of strength of concrete. The hatched area indicates the heating-rate dependent strength valley zone. In case of rapid heating rates in the range of 70 to 200 °C in normal concrete strength a strength valley is to observe, because in this area the phase change of the water is faster than the steam movement. Only by slow heating rates dehydration processes of the physically bound water have been completed. After that, the temperature-dependent strength of concrete has a steady development.

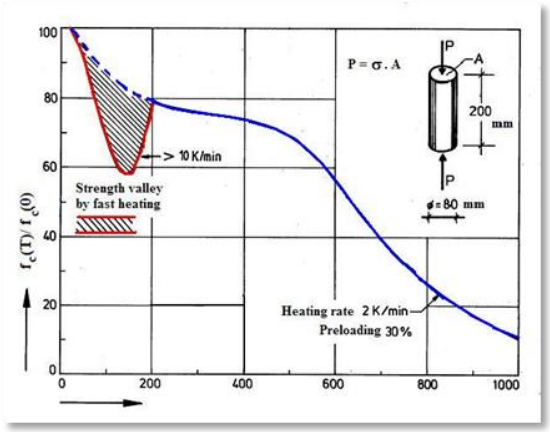

Figure 5: Related strength of concrete by elevated temperatures

In the numerical analyses the above discussed strength valley is taken into account in dependence of the heating rate. This area is regulated linearly in a temperature range of 50 to 200 °C. The consideration of a strength-valley in the calculations has initiated a significant improvement for the realistic analysis of relaxation problems at high temperatures.

Effect of Heating Rate on the Elastic Modulus of the Concrete

In accordance with the conclusions discussed in the previous subsection for the E-modulus of the concrete a similar temperature-dependent occurrence has been taken into account. Although no test results exist on an E-modulus-valley for the material concrete in a certain temperature range, it is analog assumed that the heating rate would influence the course of the modulus of elasticity respectively. This assumption is reasonable, since in many cases to estimate the modulus of elasticity the concrete strength is used.

The modulus of elasticity of the concrete is influenced not only by the temperature level attained, but also by the loading level. The related E-modulus of concrete is illustrated via temperature in Figure 6. The load level is chosen as a parameter. It is being clear that a higher load factor also causes consequent increase in modulus of elasticity. Depending on the load factor the development of the E-modulus for all temperature levels is steadily, if the heating of the structural element happens very slow.

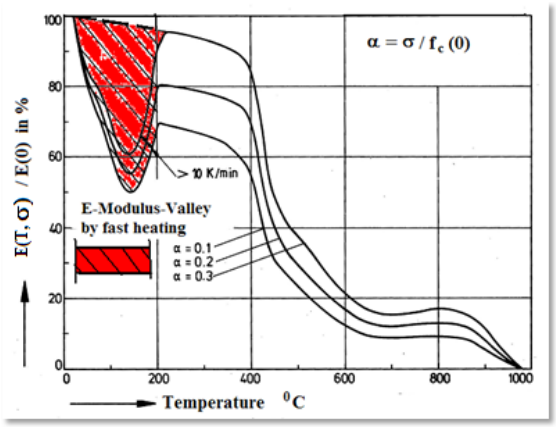

Figure 6: The related E-modulus of concrete by elevated temperatures depending on the load level.

Description of the Creep Function

The in this section presented $\bar{\varphi}$-functions were determined by extensive numerical and experimental analyses on normal concrete by the subproject B3 of SFB (**Subproject B3, 1974-1983**). The carried out theoretical investigations on large specimens have shown, however, that the thus obtained $\bar{\Phi}$-functions for normal concrete above 550 °C temperature range had to be modified. It has revealed that exceeding this temperature limit a rapid increase in the $\bar{\varphi}$-function for normal concrete should be applied. An analytical expression for the principal $\bar{\Phi}$-function can be found in **(Schneider, U., 1979).**

Influence of the load level

The experimental results show in **(Schneider, U., 1979)** that the temperature-dependent $\bar{\varphi}$-values (See Eq. 46) lie in a narrow distribution. It is however known that the modulus of elasticity of the concrete depends on both the temperature effect and also on the existing compression stress. When the results are evaluated from this point of view, then it is determined that the creep values lie no longer in a narrow zone.

The evaluated results and their development via temperature for a certain load level of $\bar{\varphi}$-values are illustrated in Figure 7. $\bar{\varphi}$-Function is shown in the figure in a set of curves, whereas parameter the moisture content in weight-percent is specified. It is determined that with increasing load factor the creep values also increase and the creep functions almost linearize (s. Figure 8). However, this property is valid up to the temperature limit of 550 °C.

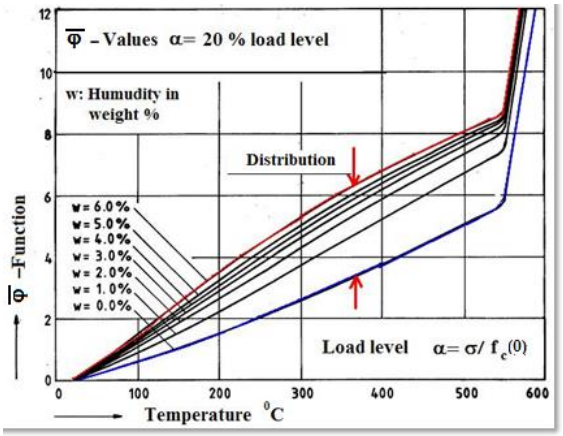

Figure 7: Creep function $\bar{\varphi}$ in case of 20 % load level

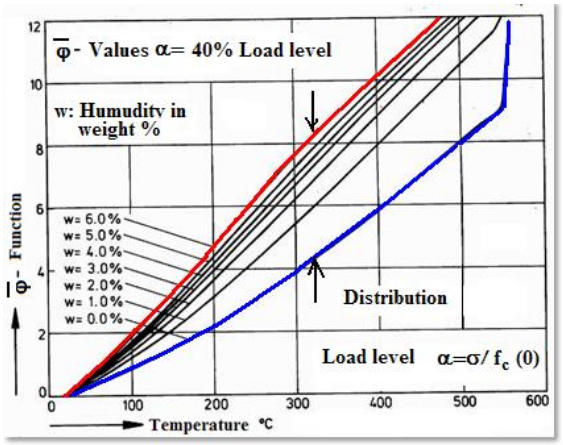

Figure 8: Creep function $\bar{\varphi}$ in case of 40 % load level

Influence of the concrete humidity on creep of concrete

Figure 9 shows the creep development for specific moisture content in the specimen. The load level has been chosen as a parameter. It will be clear that the load level apparently has a small influence in the temperature range of 20 to 500 °C on the $\bar{\Phi}$-values. In this area, the creep function is almost linear; after exceeding this limit, the linearity disappears and the load level shows its influence considerably.

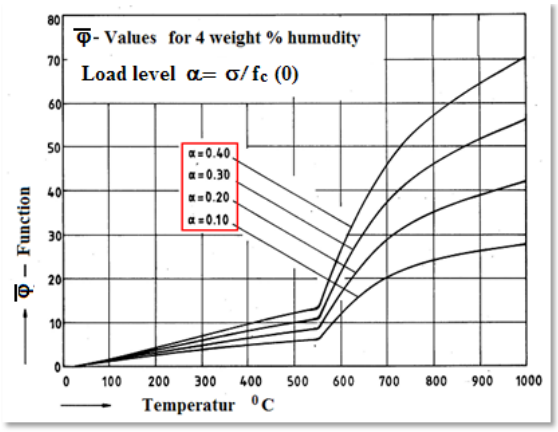

Figure 9: Creep function $\bar{\varphi}$ for 4 weight-percent concrete humidity.

Influence of stand-time

In the subsection *"Successive calculation of the compressive stresses"* it was shown that the creep function depends not only on the temperature and the load level, but must also be modified by a time parameter in order to take into account the long-term creep effects. Eq. 47 describes this characteristic of the creep function. The extensive calculations performed have shown that the creep function can be best illustrated in the way that the stress and temperature dependent effects are multiplied by an appropriate time function. These functional relationships are in Eq. 48 displayed. It also contains the geometric influence of the specimen.

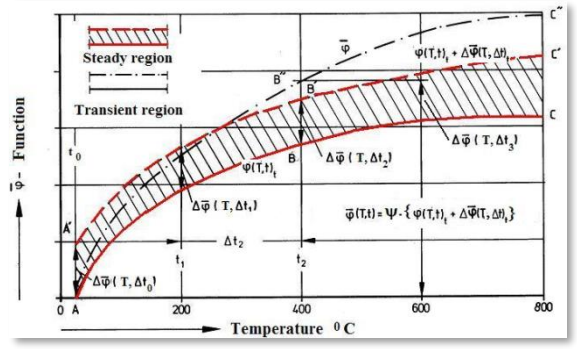

Figure 10: Influence of temperature stand-time on creep-function.

The influence of stand-time on the development of creep function is illustrated in the Figure 10 via the temperature in principle. In the figure the influences of steady and unsteady temperature effects have been made distinct. The curve A-B-C gives the basic creep-factor of a test specimen, which is heated with load up to a certain temperature, under a certain heating rate. When the temperature attained is then maintained stabile, by this additional creep deformations occur. This process is represented by a hatched area in Figure 10, which reflects the increase in the creep factors in accordance with the progressive stand-time.

The new creep function is shown in Figure 10 for a certain time Δt_1-step with the curve A'-B'-C '. In case of fire, however, unsteady temperatures are acting, so that the final creep factor is calculated successively for a specific temperature level (Eq. 49):

$$\bar{\varphi}\,(T,t) = \psi.\{\varphi(T,t)_{t-1} + \overline{\Delta\varphi}(T,\Delta t)_t\} \qquad (49)$$

The resulting new $\bar{\varphi}$-function is also shown in Figure 10 principally with the curve $A'' - B'' - C''$.

Irreversible Application for Reinforcing Steel

Extensive studies have indicated that taking into account the time effects for realistic material behavior of steel does not provide a special contribution (**Hoffend, F., 1981-1983**). Therefore, the stresses in the calculation during an acting load are non-linear-elastic determined. On the other hand a linear-elastic behavior to the building material is assigned when an unloading exists. That means a Hysteresis-Curve is applied for the stress-strain relationship for the constant steel temperature. Thus, during the cooling phase of the component temperatures, for example, remaining expansions are determined in the calculation.

SUMMARIES

It has been presented in SFB and in other research works a general calculation model for concrete materials for high temperatures. The application of these mathematical models presented has shown, however, that the material description was not complete and not enough realistic. Therefore, some models could be used successfully for certain boundary conditions. This reality is due to the fact that either experimental data have been obtained from steady state, or from unsteady temperature conditions. In some cases even partly mixed approach was applied. Numerical studies have shown that the material models that have been developed through the analysis of unsteady data are the best method to describe the material behavior in case of fire.

The results of the research works in SFB 148 showed that a material model for concrete has to include the transition creep or at least proper deformation effects. Such conditions shall in particular represent a benchmark for the fire test when a component is under restraining effects while the deformations and restraints shall be predicted and compared with test results (**Haksever, A., 1980**). The here proposed material model bases on the research works of **SFB 148**. The material model includes important premises that takes into account the transition creep and therefore for the fire protec-

tion design of reinforced concrete elements finds a reliable application also in restraining conditions.

The decisive solution of the relaxation problem was achieved by taking into account the most important physical factors *($\dot{T}$, w, σ)* in the determination of the concrete strength and the modulus of elasticity *E(T, σ)* (**Weiß, R., 1977**). Also, the modification of the creep function in consideration of the geometric shape of the test specimen and long-term time effects has been an important improvement. The validity of the model presented here will be shown in another contribution (Part II) of the author.

Ackknowledgement: The Deutscheforschungsgemeinschaft (German Research Foundation) has supported the research works of SFB, where the author was also active for many years, deserves particular thanks and appreciates.

NOTATIONS

f	Strength	[N/ mm^2]
f_c	Concrete strength	[N/ mm^2]
$f_c(T)$	Temperature dependent concrete strength	[N/ mm^2]
$f_c(0)$	Initial concrete strength	[N/ mm^2]
l	Length	[mm]
T	Temperature	[K]
$\dot{T}$	Heating rate	[K/min]
t	Time	[sec]
$E(t)$	Modulus of Elasticity for a certain time duration	[N/mm^2]
$E(0)$	Initial modulus of Elasticity	[N/mm^2]
$E(T, \sigma)$	Temperature and stress dependent modulus of Elasticity	[N/mm^2]
$\dot{E}$	Modulus of Elasticity differential by time	[N/mm^2/s]
r_s	Hydraulic radius of large specimen	[mm]
r_z	Hydraulic radius of small specimen	[mm]
w	Humidity	[%]

Additional Symbols

α	Load level
ε	Strain
ε_0	Initial strain
ε_s	Shrinkage
ε_{el}	Elastic expansion
ε_{pl}	Plastic strain
ε_{th}	Thermal expansion
ε_c	Creep deformation
ε_σ	Spontaneous stress dependent compression
ε_{tot}	Total expansion
ε_{scr}	Stationary creep
ε_{tcr}	Transient creep
φ(T, t)	Creep function
$\bar{\Phi}$(σ, T, w)	Modified creep function
$\psi(t, r_s, r_z)$	Modification factor for creep function
J(σ, t)	Function for creep deformations

σ	Stress	[N/mm^2]
σ_t	Actual stress	[N/mm^2]
σ_{t-1}	Previous stress	[N/mm^2]
$\dot{\sigma}$	Stress differential by time	[N/mm^2/s]
$\tilde{\sigma}$	Stress history	[N/mm^2]
Δt	Time increment	[s]

$\Delta\bar{\varphi}(\Delta t)$ Stationary creep increment

The other notations are defined where they appear in the text.

REFERENCES

1. Anderberg, Y.: Fire-Exposed Hyperstatic Concrete Structures - An Experimental and Theoretical Study. Div. of Struct. Mechn. and Concrete Constr., Inst, of Techn., Lund, 1976.
2. Anderberg, Y. et al.: Stress and deformation characteristics of concrete in high temperatures. Lund Inst. of Techn., Bulletin 54, Lund 1976.
3. Bazant, Z.P.: Mathematical Model for Creep and Thermal Shrinkage of Concrete at High Temperatures. Report No.82-10/249m, The Techn. Inst., Northwestern University, Evanston, 1982.
4. Bronstein-Semendjajew.; Taschenbuch der Mathematik (Handbook of Mathematic)., Teubnerverlag., Leipzig, 1973
5. Cabrita Neves, J.C. Valente, J.P. Correia Rodrigues., Thermal restraint and fire resistance of columns., Fire Safety Journal, Volume 37, Issue 8, November 2002, Pages 753-771.

6. David Lange, Johan Sjöström., Mechanical response of a partially restrained column exposed to localized fires. Fire Safety Journal, Volume 67, July 2014, Pages 82-95.
7. DIN 4102 – Brandverhalten von Baustoffen und Bauteilen Teile 1-3, Teile 5-7, and Teil 4., DIN Deutsches Institut für Normung E.V., Beuth Verlag, Berlin, (1981)
8. Ehm, C.: Versuche zur Festigkeit und Verformung von Beton unter zweiaxialer Bean-spruchung und hohen Temperaturen (Experiments on the concrete strength under biaxial loading and elavated temperatures). Dissertation, Technische Universität Braunschweig, 1985.
9. DIN V ENV 1992-1-2 Eurocode 2 – Planung von Stahlbeton- und Spannbetontragwerken, Teil 1-2: Allgemeine Regeln – Tragwerksbemessung für den Brandfall, (1997).
10. Frank Fingerloos and Ekkehard Richter., Nachweis des konstruktiven Brandschutzes bei Stahlbetonstützen., Beton- und Stahlbetonbau, (Design of the Structural Fire Protection of Reinforced Concrete Column) , (2007).
11. Haksever, A.: Relaxationsverhalten von Stahlbetontragwerken im Brandfall (Relaxation behaviour of concrete structures in case of fire). SFB 148, Research report 1978-1980, Part A1-5, TU-Braunschweig, 1980
12. Hoffend, F.; Zum Brandverhalten von Stahl-betonbauteilen., Versuchsergebnisse und rechnerische Unterschungen (On the fire behaviour of structural reinforced concrete elements and computational studies) ., SFB 148., Res. Report 1981-1983, Part I, pp 57-59.
13. Jens Upmeyer and Peter Schaumann: Zum Feuerwiderstand von Stahlbetonstützen, Beton- und Stahlbetonbau., (Fire Resistance of Reinforced Concrete Columns). (2008).
14. Jean-Marc Franssen., Failure temperature of a system comprising a restrained column submitted to fire., Fire Safety Journal, Volume 34, Issue 2, 3 March 2000, Pages 191-207.
15. Kordina. K.: The behavior of structural elements and buildings under fire. Rheinisch-Werfaelische Akademie der Wissenscahften., Nr. 281. Westdeutscher Verlag, Opladen., 1979.
16. Kordina. K., Schneider, U.: Über das Verhalten von Beton unter hohen Temperaturen (On the behavior of concrete under elevated temperatures), Betonwerk-Fertigteil-Techn. 41. Jahrg, Heft 12.
17. Michael Cyllok, and Marcus Achenbach. Bemessung von Stahlbetonstützen im Brandfall: Absicherung der nichtlinearen Zonenmethode durch Laborversuche., Beton- und Stahlbetonbau., Design of Reinforced Concrete Columns exposed to Fire: Validation of Simplified Method (Zone Method) by Tests., (2011)
18. Schneider, U.: Properties of Materials at High Temperatures - Concrete -. RILEM 44-PHT, University of Kassel, Kassel, 1985.
19. Schneider, U.: Behaviour of Concrete at High Temperatures. Deutscher Ausschuß für Stahlbeton, Heft 337, Verlag W. Ernst und Sohn, Berlin, 1982.
20. Schneider, U.: Design of structures against fire, Symposium, The University of Aston, Birmingham, April 15-16, 1986.
21. Schneider, U.: Ein Beitrag zur Frage des Kriechens und der Relaxation von Beton unter hohen Temperaturen (A contribution to the question of creep and relaxation of concrete in elevated temperatures). (Habil. -Work.), 1979. SFB 148., Subproject B3., Research Report., 1974-1983.
22. Schneider, U.: Zur kinetik festigkeitsmindernder Reaktionen in Normalbetonen bei hohen Temperaturen., (On the kinetic of strength lessening reactions in normal concrete in elevated tempe-ratures). Diss. TU-Braunschweig, 1973.
23. SFB 148.: "Sonderforschungsbereich 148; Brandverhalten von Bauteilen" (A special research field Nr. 148; Fire response of structural elements). Technisce Universität Braunschweig., Germany., (1971-1986)
24. Sven Huismann, Manfred Korzen, Andreas Rogge., Entwicklung und Validierung eines allgemeinen Rechenverfahrens für Stahlbetonstützen aus hochfestem Beton unter Brandbeanspruchung., (Development and Validation of an Advanced Calculation Model for High Strength Concrete Columns Subjected to Fire Loading).,Beton- und Stahlbetonbau, (2012).
25. Truong-Thang Nguyen, Kang Hai Tan., Thermal-induced restraint forces in reinforced concrete columns subjected to eccentric loads. Fire Safety Journal, Volume 69, October 2014, Pages 136-146.
26. Ulrich Quast, Spannungsabhängige und thermische Dehnungen (Stress and thermal dependant expansions), Beton- und Stahlbetonbau, (2009).
27. Waubke, N.V.; Schneider, U.: Tensile Stresses in concrete due to fast vapor flow. -Int. symp. on pore struct, and prop of mat., Part III, Vol. V. Prag 1973.
28. Waubke, N.V.: Über einen physikalischen Gesichtspunkt der Festigkeitsverluste von Portlandzementbetonen bei Temperaturen bis 1000 °C (From the physical point of view of strength loss for Portland cement concretes in 1000 °C temperatures), -Publications of 148, Issue 2, TU-Braunschweig, Nov. 1973.
29. Waubke, N.V.; Schneider, U.: Tensile Stresses in concrete due to fast vapour flow. -Int. symp. on pore struct, and prop of mat., Part III, Vol. V. Prag 1973.
30. Weiß, R.: Ein haufwerktheoretisches Modell der Restfestigkeit geschädigter Betone (A theoretical model for residual strength of damaged concretes in pile condition), -Diss. TU-Braunschweig, 1977.
31. Yu-ye Xu, Bo Wu., Fire resistance of reinforced concrete columns with L-, T-, and +-shaped cross-sections. Fire Safety Journal, Volume 44, Issue 6, August 2009, Pages 869-880.

http://dergipark.ulakbim.gov.tr/tujes
Trakya University Journal of Engineering Sciences, 16(2): 55-60, 2015
ISSN 2147–0308
Araştırma Makalesi / Research Article

NUMERICAL STUDY OF PRESSURE DROP IN THE HORIZONTAL SPIRALLY COILED TUBES

Omid SEYEDASHRAF

Department of Civil Engineering, Kermanshah University of Technology,
67178 Pardis St., Kermanshah, Iran.
o.seyedashraf@kut.ac.ir

Abstract: Flow characteristics of spirally coiled tubes in terms of their secondary flow and pressure drop are investigated. Four spirally coiled tubes with different curvature ratios; under constant wall temperature, are numerically simulated. In the system, water is entering the innermost turn and flows out at the outermost turn. To build the numerical model, a finite volume method with an unstructured grid system is employed for solving the Navier-Stokes equations system. Correspondingly, the standard k–ε turbulence model is employed to predict the flow development. Here, the mass flow rate in the spirally coiled tube is set to vary within the range 0.03-0.12 kg/s. The numerically obtained data of the pressure drop in the spiral coils are put side by side the experimental data reported in the literature. A close agreement is observed between the experimental data and the results of this study. Based on the results, a new correlation is proposed for predicting the pressure drop in horizontal spiral coils.

Keywords: Coil, Spirally Coiled Tube, Pressure Drop, Finite Volume Method, Standard k–ε

INTRODUCTION

Spiral coils are regularly used curved tubes, which have been utilized in a wide variety of engineering applications such as heating, refrigerating systems, HVAC systems, steam generator and condensers in power plants and chemical reactors. In a curved tube, because of the differences between the inertial and centrifugal forces, a secondary flow originates in the cross section of the pipe. The heat transfer and flow developments in these tubes significantly depend on the performance of the induced secondary flow.

Flow and heat transfer in spiral pipes with circular or rectangular cross-section has been a topic of important fundamental engineering interests during the past decades. Orlov and Tselishchev (1964), illustrated an experimental research on heat transfer from spiral and helical coils with a turbulent water flow. They proposed a correlation to predict the inside heat transfer coefficient of spiral coils.

Ho et al. (1995 & 1999) employed correlations of the tube-side and air-side heat transfer coefficients to define the thermal functioning of the spiral-coil heat exchanger under cooling and dehumidifying conditions. Experimental benchmarks were evaluated to verify the results. Nakayama et al. (2000), studied the cooling potentialities of a fluid fluxing through a spiral coil, which was drowned in a cold water container. Accordingly, an axisymmetric mathematical scheme was invented and proposed to assess the temperature of the fluid in a spiral coil and that of the surface of the coil. Naphon and Wongwises (2002), reported an experimental survey on in-tube convective heat transfer coefficients in a spiral coil heat exchanger. The heat exchanger was made of six layers of homocentric spirally coiled tubes, each with five turns. The effects of relevant parameters were investigated. They proposed a novel formula based on their experimental data to simulate and predict in-tube heat transfer coefficient of spiral coils. Naphon and Wongwises (2003 & 2005), modified the mathematical model of Ho et al. (1995), by considering the fin efficiency and using the other accessible heat transfer coefficient correlations to prescribe the flow characteristics and heat transfer attributes of spiral coil tube heat exchanger subjected to wet-surface environment. The relevant parameters on the performance of the heat exchanger were discussed.

Naphon and Suwagrai (2007), experimentally and numerically investigated the heat transfer and flow developments in the horizontal spirally coiled tubes. They compared the heat transfer and pressure drop of a spirally coiled tube side by side those from the straight ones and compared them. It was revealed that because of the existence of centrifugal force, the pressure drop and Nusselt number acquired from the spirally coiled tube were 1.49, 1.50 times higher than the ones obtained from the straight tube, respectively. Mittal et al. (2009), using a mathematical model investigated the adiabatic flow of a refrigerant fluid through a spiral capillary tube making use of a homogenous model together with the metastable liquid. Lee et al. (2010), considered the air-side heat transfer properties of spiral-type circular fin-tube heat exchangers used as evaporators in household refrigerators. Moreover, Yoo et. al. (2012), numerically investigated the flow characteristics of spirally coiled tubes making use of the state of the art Fluent CFD package. Different geometries with various Reynolds numbers were evaluated and was concluded that the Reynolds number following with the Nusselt number and friction factor have a stronger

effect compared to the curvature ratio of the spirally coiled tubes.

Though some investigations have been performed on performance and in-tube heat transfer of spiral coils, no thorough work has been reported on the pressure drop. The objective of this study is to obtain a correlation to determine the pressure drop for the steady state flow in horizontal spiral coils.

GEOMETRY OF SPIRALLY COILED TUBES

A scheme of a typical spirally coiled tube is presented in Figure 1. In this figure, *b* is the coil pitch and R_{min} and R_{max} are the minimum and maximum curvature radii, respectively. The curvature radius of a spiral coil, R_c, is defined as:

$$R_c = \frac{R_{\min} + R_{\max}}{2} \tag{1}$$

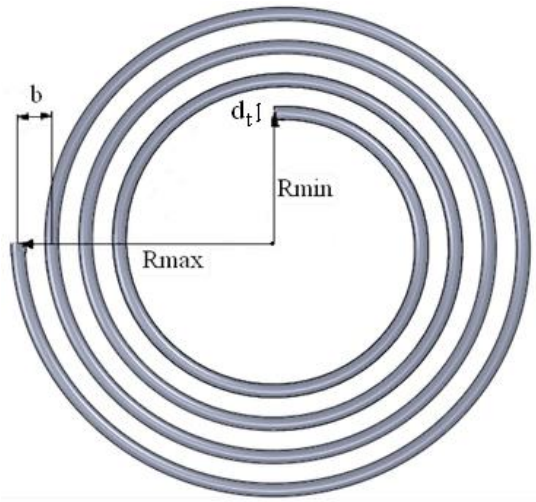

Figure 1. Schematic of a spiral coil

The geometrical specifications of the four coils that were used in the numerical study are given in Table 1.

Table 1. Coil Dimensions

Coil	R_{max} (mm)	R_{min} (mm)	d_t (mm)	b (mm)
1	250	100	10	50
2	200	125	10	25
3	172	82	8.025	18
4	136	82	8.025	18

MODEL DESCRIPTION

Governing Equations

The standard k–ε model is utilized to simulate the turbulent flow and heat transfer developments. Here, the governing equations are based on the conservation of mass, momentum, and energy. A state of the art CFD code is employed, which uses the finite volume method to transfer the continuous equations into discretized ones by integration of the governing equation over the control volumes and eventually solve the linearized equations. The governing equations are defined as:

$$\frac{\partial(\rho)}{\partial t} + \frac{\partial(\rho u_i)}{\partial x_i} = 0 \tag{2}$$

$$\frac{\partial(\rho u_i)}{\partial t} + \frac{\partial(\rho u_i u_j)}{\partial x_j} = \frac{\partial \tau_{ij}}{\partial x_j} - \frac{\partial p}{\partial x_i} \tag{3}$$

$$\frac{\partial(\rho E)}{\partial t} + \frac{\partial(\rho u_j E)}{\partial x_j} = \frac{\partial}{\partial x_j}\left(k \frac{\partial T}{\partial x_j}\right) + \frac{\partial(\tau_{ij} u_j)}{\partial x_j} \tag{4}$$

where t is time, u_i is the i-th component of the Reynolds averaged velocity, x_i the i-th axis (with the axis x_3 vertical and oriented upward), ρ is the water density, P is the Reynolds averaged pressure and g is the acceleration due to gravity.

In a Newtonian fluid τ_{ij} is calculated as follows:

$$\tau_{ij} = \mu\left[\left(\frac{\partial u_i}{\partial x_j} + \frac{\partial u_j}{\partial x_i}\right) - \frac{2}{3}\frac{\partial u_k}{\partial x_k}\right] \tag{5}$$

The non-equilibrium wall-function treatment was adopted and the standard k-ε turbulence model, as the most robust, economical, reasonably accurate and long accumulated performance data, was included in the equations system.

The turbulent kinetic energy k, and the turbulent kinetic energy dissipation ε, are coupled to the main governing equations via the turbulent viscosity relation. Here, the equation for k contains additional turbulent fluctuation terms that are unidentified. Using the bossiness assumption, these fluctuation terms can be linked to the mean flow.

$$\frac{\partial(\rho k)}{\partial t} + div(\rho k \mathbf{U}) = div\left[\frac{\mu_t}{\sigma_k} grad\ k\right] + 2\mu_t E_{ij}.E_{ij} - \rho\varepsilon \tag{6}$$

$$\frac{\partial(\rho\varepsilon)}{\partial t} + div(\rho\varepsilon \mathbf{U}) = div\left[\frac{\mu_t}{\sigma_\varepsilon} grad\ \varepsilon\right] + C_{1\varepsilon}\frac{\varepsilon}{k}2\mu_t E_{ij}.E_{ij} - C_{2\varepsilon}\rho\frac{\varepsilon^2}{k} \tag{7}$$

where U is the velocity vector, E_{ij} is the mean rate of deformation tensor, $C_{1\varepsilon}$ and $C_{2\varepsilon}$ are constants, and typical values of 1.44 and 1.92 are used. In these equations, the Prandtl number σ_k connects the diffusivity of k to the eddy viscosity and normally a value of 1.0 is used. Moreover, the Prandtl number σ_ε connects the diffusivity of ε to the eddy

viscosity and generally a value of 1.30 is used (Seyedashraf and Akhtari, 2016).

Boundary Conditions

The boundary conditions implemented in this study are as follows: the water inlet is defined as velocity-inlet, outflow boundary conditions are used to model the flow exit; since the details of the flow velocity and pressure are not known prior to solution of the flow problem. Additionally, the no-slip wall boundary condition in conjunction with a constant wall temperature T_w, as the thermal boundary condition was imposed on the spirally coiled tube wall.

Initial Conditions

At the inlet boundary condition, the uniform profiles of all the properties are considered, as follows:

$$u = u_{in},\ v = 0,\ w = 0,\ k = k_{in},\ \varepsilon = \varepsilon_{in} \tag{8}$$

The turbulent kinetic energy k_{in}, and the turbulent kinetic energy dissipation ε_{in}, at the inlet section are approximated from the turbulent intensity I, and a turbulent characteristics length L, as follows:

$$k_{in} = \frac{3}{2}(u_{in} I)^2, \quad \varepsilon_{\text{in}} = \frac{C_{\mu}^{3/4} k_{\text{in}}^{3/2}}{L} \tag{9}$$

The turbulence characteristic length L, is set to $0.07r$ (Versteeg and Malalasekera, 1995).

Numerical Modeling

The three-dimensional flow domain was divided into numbers of non-overlapping unstructured mesh with 505112 hexahedral segments and 527175 nodes. Out of different possible meshing schemes, the chosen form is suitable for both accuracy and the time duration of the convergence. The unstructured non-uniform grid system is shown in Figure 2.

The employed CFD code uses the finite volume method in conjunction with a coupling technique, which simultaneously discretizes and solves transport equations in the whole domain through a false time-step algorithm. Convection terms are linearized using third order monotone upstream centered scheme for conservation law (MUSCL) (Van Leer, 1976). The linearized system of equations is preconditioned in order to reduce eigen-values to the same order of magnitude. Pressure-implicit with splitting of operators (PISO) method was employed to deal with the problem of velocity and pressure coupling (Oliveira and Issa, 2001). PISO methods incorporate pressure effect through momentum equations into the continuity equation to obtain correction equations for pressure.

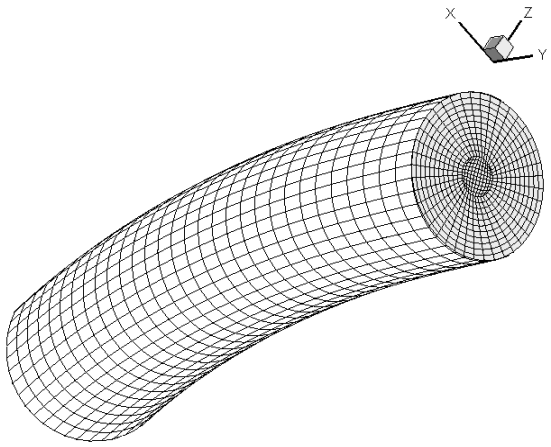

Figure 1. Grid form used to perform the computations.

2500 iterations for each simulation was reached in this study for a full convergence. The unstructured grid approach here has significantly enhanced the speed of convergence.

The conditions that were used in numerical study are given in Table 2.

Table 2. Employed variables in the CFD analysis

Variable	Range
Inlet water temperature, K	293
Wall temperature, K	320
Water flow rate, kg/s	0.03-0.12

RESULTS AND DISCUSSION

A numerical study for flow fields was conducted on a horizontal spiral coil, using water as the working fluid. Comparing the numerically obtained results it was concluded that the finite volume method in conjunction with the standard k-ε turbulence model has the capability of capturing specific flow behaviors in spiral coils. Figure 3 shows the development of axial velocity at different cross-sections (φ= 90°, 180°, 360°, 720°) for coil #1 at Re=38500. As depicted in this figure, when the axial distance is small, the secondary flow would become weak. Due to the effect of centrifugal forces, the flow in the core of the pipe begins to be forced to the outer section of the bend. Moreover, as the φ parameter increases, the secondary velocity enhances and the high axial velocity zone shifts to the outer side, as shown in this figure.

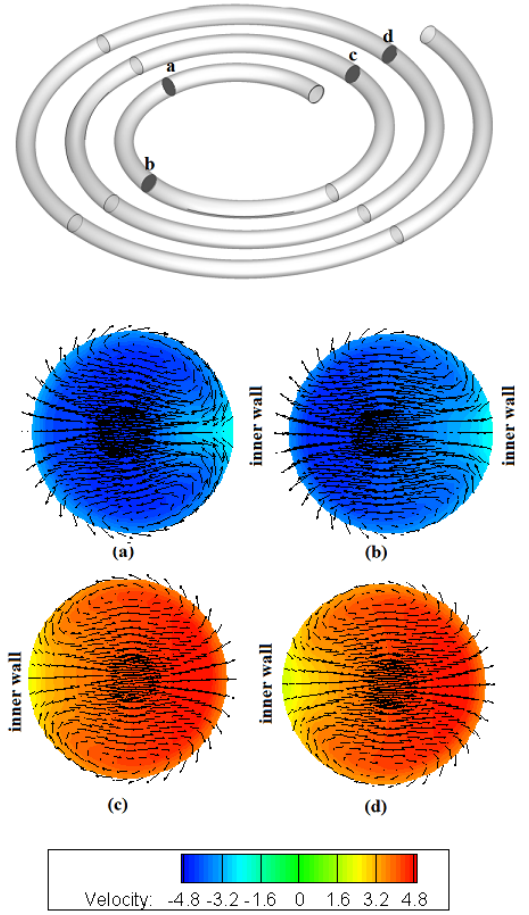

Figure 3. Velocity fields and vectors of water flow in a spirally coiled tube and different sections: (a)φ=90°, (b)φ=180°, (c)φ =360°, (d)φ =720°

Accordingly, the form of the secondary flow would depend on the axial distance from the inlet section. Figure 4 demonstrates the longitudinal pressure contours along the tube.

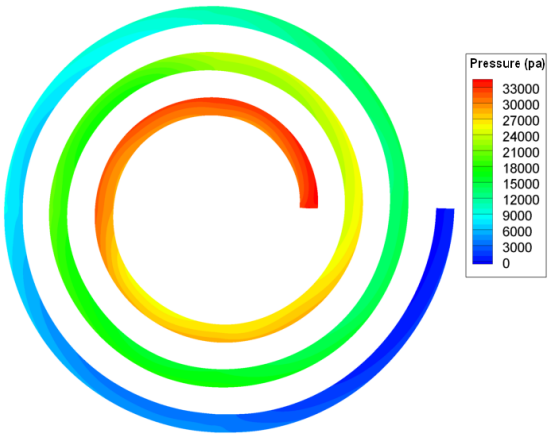

Figure 4. Pressure contours (pa).

Analysis of the Numerical Data

For flow in spiral coils, pressure drop ΔP, as a dependent variable, depends on the independent variables of the fluid properties (ρ and μ), the inlet velocity (u), and the parameters of the coil geometry (R_{min}, R_{max}, b, d_t). Thus:

$$\Delta P = f(\rho, \mu, u, R_{\min}, R_{\max}, b, d_t) \tag{10}$$

To obtain a correlation for pressure drop in spiral coils the form $EuG = \alpha Re^{\beta}$, which is the same form as that of Hagen–Poiseuille law $Eu(d/L)=16/Re$, and Blasius resistance law $Eu(d/L)=0.0791Re^{-0.25}$, has been used. Where $Eu=\Delta P/(0.5\rho u^2)$ is the Euler number and G is some geometrical dimensionless group, which depends on the geometry of the coil. This form of correlation has been used by some researchers for pressure drop in helical and spiral coils (Shaukat and Seshadri, 1971, Shaukat and Zaidi, 1979, Srinivasan, et al. 1968, Ramana and Sadasivudu, 1974, Dyke, 1978).

Shaukat (2001) developed a correlation for pressure drop in helical coil tubes, as follows:

$$EuGrhc = 0.09Re^{-1/5} \quad , \quad Re > 1000 \tag{11}$$

where *Grhc* is an appropriate geometrical parameter of helical coil.

Since the flow patterns; due to secondary flow of spiral coils are similar to those of helical coils, in this study, the pressure drop predicting correlation is considered as follow:

$$EuG = Re^{-1/5}$$

in which the power of Reynolds number is considered to be similar to the correlation of Shaukat (2001). In Eq. (12) the geometrical dimensionless parameter *G*, must be defined for a spiral coil.

Based on the numerical results attempts were made to obtain the best correlation for *G*, resulted in a relationship as follows:

$$G = 0.007\left(\frac{R_{\max}+R_{\min}}{R_{\max}-R_{\min}}\right)^{-0.757}\left(\frac{d_t}{b}\right)^{-1.252} \tag{13}$$

Therefore, Eq. (12) can be written as:

$$Eu\left[\left(\frac{R_{\max}+R_{\min}}{R_{\max}-R_{\min}}\right)^{-0.757}\left(\frac{d_t}{b}\right)^{-1.252}\right] = 142.86\,\mathrm{Re}^{-1/5}$$

$$7000 < Re < 17000 \tag{14}$$

The predicted results for pressure drop in horizontal spiral coiled tubes are compared with the experimental data presented by Naphon and Suwagrai (2007). Figure 5 indicates the computed pressure drop against the respective experimental values.

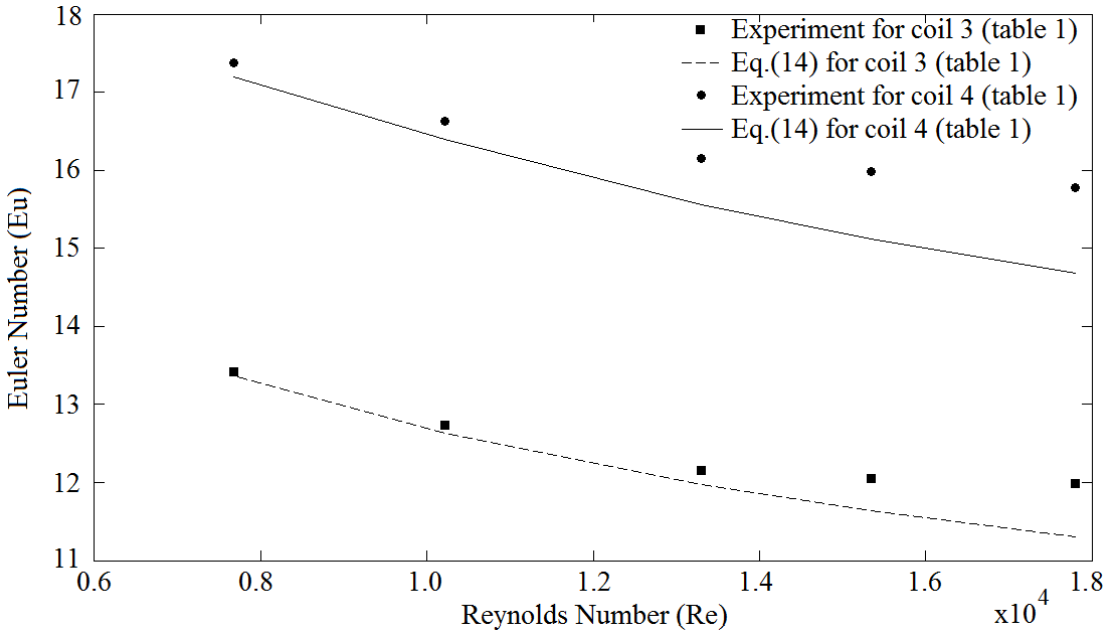

Figure 5. The Euler number computed by CFD (Eq. 14) against the experimental values of Naphon and Suwagrai (2007).

As it can be observed from the figure, there is a reasonable agreement between the numerical and experimental values. The largest discrepancies are obtained for the large mass flow rates, corresponding to the largest Reynolds number. The average and maximum deviations of Eq. (14) with the experimental data for the coil 3 and 4 (Table 1) are 6.27% and 11.05% respectively.

REFERENCES

1. Dyke, M.V., Extended Stokes series laminarflow through a loosely coiled pipe, Journal of Fluid Mechanics, 86(1): p. 129–145, 1978.
2. Ho J.C., Wijeysundera, N.E., and S. Rajasekar, An unmixed-air flow model of a spiral cooling dehumidifying heat transfer. Applied Thermal Engineering, 19(8): p. 865–883, 1999.
3. Ho, J.C., Wijeysundera, N.E., Rajasekar, S., and T.T. Chandratilleke, Performance of a compact spiral coil heat exchange. Heat Recovery Syst. and CHP, 15(5): p. 457–468, 1995.
4. Lee, M., Kang, T. and Y. Kim, Air-side heat transfer characteristics of spiral-type circular fin-tube heat exchangers, international journal of refrigeration, 33(2): p. 313–320, 2010.
5. Mittal, M.K., Kumar, R. and A. Gupta, Numerical analysis of adiabatic flow of refrigerant through a spiral capillary tube, International Journal of Thermal Sciences, 48(7): p. 1348–1354, 2009.
6. Nakayama, A., Kokubo, N., Ishida, T., and F. Kuwahara, Conjugate numerical model for cooling a fluid flowing through a spiral coil immersed in a chilled water container, Numer. Heat Transfer: Part A, 37(2): p. 155–165, 2000.
7. Naphon, P., and J. Suwagrai, Effect of curvature ratios on the heat transfer and flow developments in the horizontal spirally coiled tubes, International Journal of Heat and Mass Transfer, 50(3): p. 444–451, 2007.
8. Naphon, P., and S. Wongwises, An experimental study on the in-tube heat transfer coefficients in a spiral-coil heat exchanger, International Communications in Heat and Mass Transfer, 29(6): p. 797–809, 2002.
9. Naphon, P., and S. Wongwises, A study of the heat transfer characteristics of a compact spiral coil heat exchanger under wet-surface conditions, Experimental Thermal and Fluid Science, 29(4): p. 511–521, 2005.
10. Naphon, P., and S. Wongwises, Investigation of the performance of a spiral-coil finned tube heat exchanger under dehumidifying conditions, Journal of Engineering Physics and Thermophysics, 76(1): p. 83–92. 2003
11. Oliveira, P.J., and R.I. Issa, An Improved PISO Algorithm for the Computation of Buoyancy-Driven Flows, Numerical Heat Transfer, 40(6): p. 473-493, 2001.
12. Orlov, V.K., and P.A. Tselishchev, Heat exchange in spiral coil with turbulent flow of water. Thermal Engineering. (Translated from Teploenergetika), 11(12): p. 97-99, 1964.
13. Ramana Rao, M.V., and D. Sadasivudu, Pressure drop studies in helical coils, Indian journal of technology, 12(1): p. 473-479, 1974.
14. Seyedashraf, O., and A.A. Akhtari, Flow separation control in open-channel bends, Journal of the Chinese Institute of Engineers, 39(1): p.40-48, 2016.

15. Shaukat, A., Pressure drop correlations for flow through regular helical coil tubes, J. Fluid Dynamic Research, 28(4): p. 295-310, 2001.

16. Shaukat, A., and C.V. Seshadri, Pressure drop in Archimedean spiral tubes, Industrial & Engineering Chemistry Process Design and Development, 10(3): p. 328–332, 1971.

17. Shaukat, A., and A.H. Zaidi, Head loss and Critical Reynolds Numbers for Flow in ascending equiangular spiral tube coils, Industrial & Engineering Chemistry Process Design and Development, 18(2): p. 349–353, 1979.

18. Srinivasan, P.S., Nandapurkar, S.S. and F.A. Holland, Pressure drop and heat transfer in coils, Transactions of the institution of chemical engineering and the chemical engineer, 46(4), 1968.

19. Van Leer, B., MUSCL, A New Approach to Numerical Gas Dynamics, in Computing in Plasmaphysics and Astrophysics, in Proceedings of the Second European Conference on Computational Physics. Max-Planck-Institut fur Plasmaphysik, Garching, 1976.

20. Versteeg, H.K., and W. Malalasekera, Computational Fluid Dynamics, Longman Group, (1995).

21. Yoo, G. J., Choi, H. K., and W.R. Dong, Fluid flow and heat transfer characteristics of spiral coiled tube: Effects of Reynolds number and curvature ratio, Journal of Central South University, 19(2): p. 471−476, 2012.

http://dergipark.ulakbim.gov.tr/tujes
Trakya University Journal of Engineering Sciences, 16(2): 61-69, 2015
ISSN 2147–0308
Araştırma Makalesi / Research Article

THE EFFECTS OF GEOTEXTILE LAYERS ON BEARING CAPACITY OF GRAVEL-SILT MIXTURES

Keramat SADEGHI AZAR[1], Rouzbeh DABIRI[2]

[1]Department of Engineering Geology, Ahar Branch, Islamic Azad University, Ahar, Iran
[2]Department of Civil Engineering, Tabriz Branch, Islamic Azad University, Tabriz, Iran
Corresponding author's email: rouzbeh_dabiri@iaut.ac.ir

Abstract: Soil stabilization methods to modifying and improving the physical and engineering features of the soil for achieving a set of previously determined goals. In many engineering applications, the use of geotextiles is regarded as an effective method for soil improvement. Research results indicate that, when geosynthetics placed between the subgrade and sub base layers, increase the bearing capacity in fine grain subgrades. The main purpose of the present study was evaluating a laboratory study of the effect of geotextile layer and its number of layers on the bearing capacity of the gravel of Til region of Shabestar city, which includes 15 to 30 percent of silt. It should be noted that the mentioned tests were performed in three relative densities of 90, 95, and 100%, and the effect of geotextile layer was studied in two positions. In the first position, one geotextile layer was placed in the middle part of the soil sample, and in the second position two geotextile layers were alternatively placed in the samples. The results of laboratory studies show that putting one geotextile layer in samples helps modify and improve the bearing capacity. This increases were observed in the gravel and the gravel with 30% silt. However, putting two geotextile layers in the soil alternatively decreases resistance and bearing capacity of the samples.

Keywords: Gravel, Silt, California Bearing Ratio (CBR) Test, Soil Stabilization

Jeotekstil Tabakalarının Çakıl-Silt Karışımlarının Taşıma Kapasitesi Üzerindeki Etkileri

Özet: Toprak stabilizasyonu önceden belirlenmiş hedeflere ulaşmak için toprağın fiziksel ve mühendislik bir dizi özelliklerini değiştirmek ve geliştirmek anlamına gelir. Birçok mühendislik uygulamalarında, jeotekstil kullanımı toprak ıslahı için etkili bir yöntem olarak kabul edilir. Araştırma sonuçları, geosentetik alt zemin ve alt taban katmanları arasına yerleştirildiğinde, ince taneli zeminin dayanma kapasitesini artırmak ta olduğunu göstermektedir. Bu çalışmanın temel amacı, bir laboratuvar çalışma da jeotekstil tabakasının etkisi çakıl kapasitesine ve katmanların sayısını değerlendirmektir. %15 ila 30 oranında silt içeren çakıllar, Şebister şehrinin Till bölgesinden elde edilmiştir. Denemeler üç farklı (%90, 95 ve 100) göreceli yoğunlukta gerçekleştirilmiş ve jeotekstil tabakanın etkisi iki farklı konumda incelenmiştir. İlk pozisyonda, bir jeotekstil tabakası toprak numunesinin orta kısmında yerleştirilmiş ve ikinci konumda iki jeotekstil tabakası alternatif olarak toprak numunesine konulmuştur. Laboratuvar çalışmalarının sonuçları numunelere bir jeotekstil tabakası konulmasının taşıma kapasitesinin geliştirmesine yardımcı olduğunu göstermiştir. Meydana gelen artışlar, çakıl ve % 30 silt içeren çakılda gözlenmiştir. Ancak, toprak içine alternatif olarak iki jeotekstil katmanı koyulması numunelerin taşıma kapasitesi ve direncini azaltmaktadır.

Anahtar kelimeler: Çakıl, Silt, Kaliforniya Taşıma Oranı (CBR) Deneyi, Toprak Stabilizasyonu

INTRODUCTION

Road pavement, as a part of road structure, has a very important role in road performance and in constructing safe and smooth surfaces. Subgrade layer of the road can be compacted layer of dyke, the available natural or corrected soil. Material of subgrade is prepared according to geotechnical properties and the first layer of the pavement is built over it. Subgrade which is ultimately considered as the pavement foundation and tolerates the entire load from the pavement body and the vehicles. Therefore, making pavements with high bearing capacity and life duration as well as keeping them in suitable functioning conditions is of utmost importance. Pavement body is usually composed of several layers including the subgrade, sub-base, base and asphalt (Yoder and Witczak, 1975). The first attempts for soil improvement were made long ago by putting tree branches and leaves in the marshlands and sand plains. After a while, with putting the tree branches and leaves, a mass was formed around them and the bearing capacity of the soil increased. As a result, the mentioned places could be used as passages used for passing through. In late 1940's and 1950's, geo-synthetics were used in America, and in 1970's their use became widespread in Europe. Different types of geosynthetic materials include: geotextiles, geogrides, geonets, geomembranes, geopipes, and geocomposites. Resl and Werner (1986) conducted a laboratory study on un-weaved geotextile layer in asymmetric loading conditions. The results of their study indicated that the geotextile layer between the soil bed and sub base can increase the bearing capacity of the soft soil subgrade. Fannin and Sigurdsson (1996) conducted a study at real scales on the pavement and geotextile layers. The results of their study indicated that geotextile layer increases the loading capacity of the pavement layers. In this regard, the studies by Bergado et al. (2001), Raymond and Ismail (2003), Park and Tan (2005), Yetimoglu and Salbas

(2003), Patra et al. (2005), and Varuso et al. (2005) can be mentioned. Regarding the bearing capacity of the improved soils, and the bearing capacity of the armed soils, the studies by Haeri et al. (2000), Zhang et al. (2005), Latha and Murthy (2007), and Williams and Okine (2008), Naeine et. al (2008 AND 2009) and Senthil Kumar et al. (2012) can be mentioned. The main purpose of the present research was laboratory study of the effect of the number of geotextile layers on the bearing capacity of the gravel materials containing 15 and 30% silt. It should be mentioned that California Bearing Capacity (CBR) test was done in three relative densities of 90, 95, and 100 percent, and the effect of geotextile was studied by putting one geotextile layer in the middle of the soil sample and two geotextile layers in distances of one third in the soil sample.

MATERIALS AND METHODOLOGY

As already mentioned, the purpose of the present study was examining the effect of the number of geotextile layers on the bearing capacity of the grained soils containing 15 and 13% silt using California Bearing Ratio (CBR) Test. To achieve the mentioned purpose, it was necessary to identify the geotechnical properties of materials and the physical features the geotextiles. Finally, the laboratory equipment used in the study were described (Gohari et al.,2010).

In the present study, the gravel and silt in Til region of Shabestar City was used (Figure 2). The gravel in this area is sub angular type since its length is three times as much as its width, and it is wedge-shaped. The chemical analysis of the mentioned materials by ASTM C25 standard shows that their amount of lime is so little, but the amount of iron is high, and the utilized materials do not contain organic materials. The grading of the gravel containing 15% silt, the gravel containing 30% silt, and pure silt was determined using ASTM D421 and ASTM D422, which are shown in Figure 1 (Sadeghi azar et al., 2010).

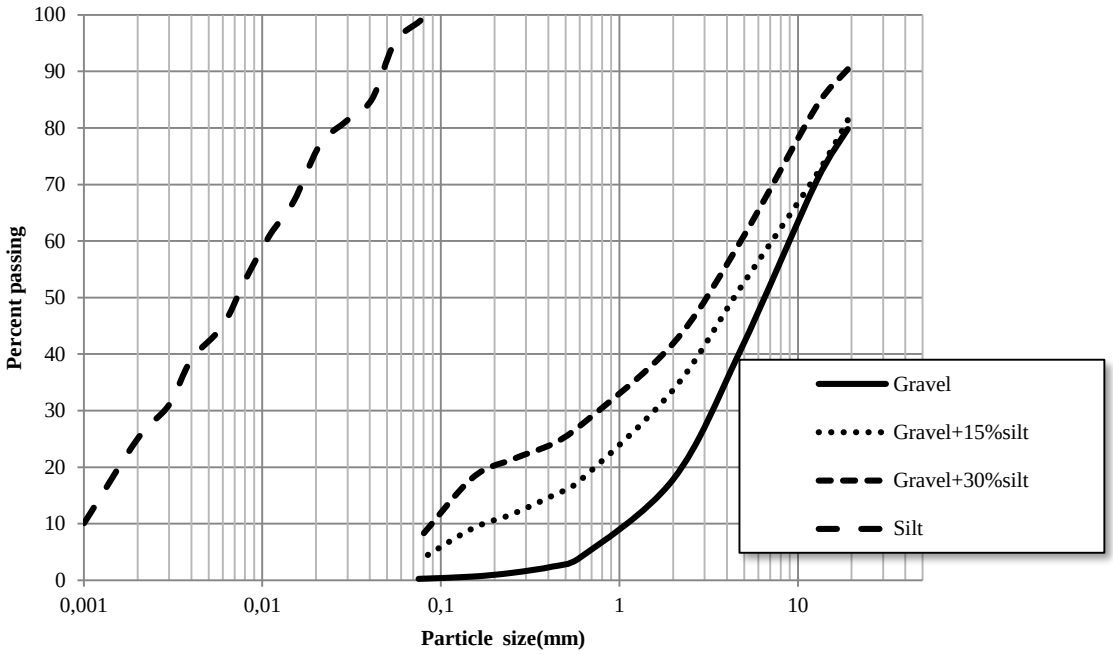

Figure 1. Grain size distribution for soils used in this study (Sadeghi azar et al., 2010).

Figure 2. Position of Til (mine of material) west of Shabestar City (www.earthgoogle.com)

As shown in Figure 1, the Gravel is in accordance with unified classification in group GW, and the silt is ML. The uniformity coefficient is C_U=9>4, indicating good grading gravel. Moreover, curvature coefficient is obtained by Cc=0.69. The Atterberg limit of the silt was PI=5 according to ASTM D4318-95a. Moreover, the values of special weight (Gs) of the materials was determined by ASTM D854 standard as given in Table 1. According to the results of XRD test, the gravel under study had a very low amount of lime, a high amount of quartz, and a little clay. The clay minerals included Kaolinites and illites. The geotextiles used in the study is one of the modern geotextiles used in geosynthetics (Secutex) industry, which is made of completely artificial fabric for long term resistance and is of un-weaved needled type. The geotextile mechanical properties used in the study are given in Table 2 (Sadeghi azar et al., 2010).

In the present study, California Bearing Ratio (CBR) were used for the tests. These tests were conducted based on ASTM D1883. Also, compaction test was performed on material according to ASTM D 698. The results of compaction tests are shown in diagrams of Figure 3.

Table 1. Specific gravity of materials in this study (Sadeghi azar et al. 2010)

Material	Gravel	Gravel+ 15%Silt	Gravel+ 30%Silt	Silt
Gs	2.72	2.68	2.6	2.63

Table 2. Engineering and index properties of geotextile reinforcement (Sadeghi et. al, 2010)

Properties	Values
Weight (g/m^2)	163
Thickness (mm)	0.9
Static puncture (CBR-test) N	2200
Dynamic cone drop (mm)	28
Tensile strength(kN/m)	15
Elongation at peak stress (%)	45-55

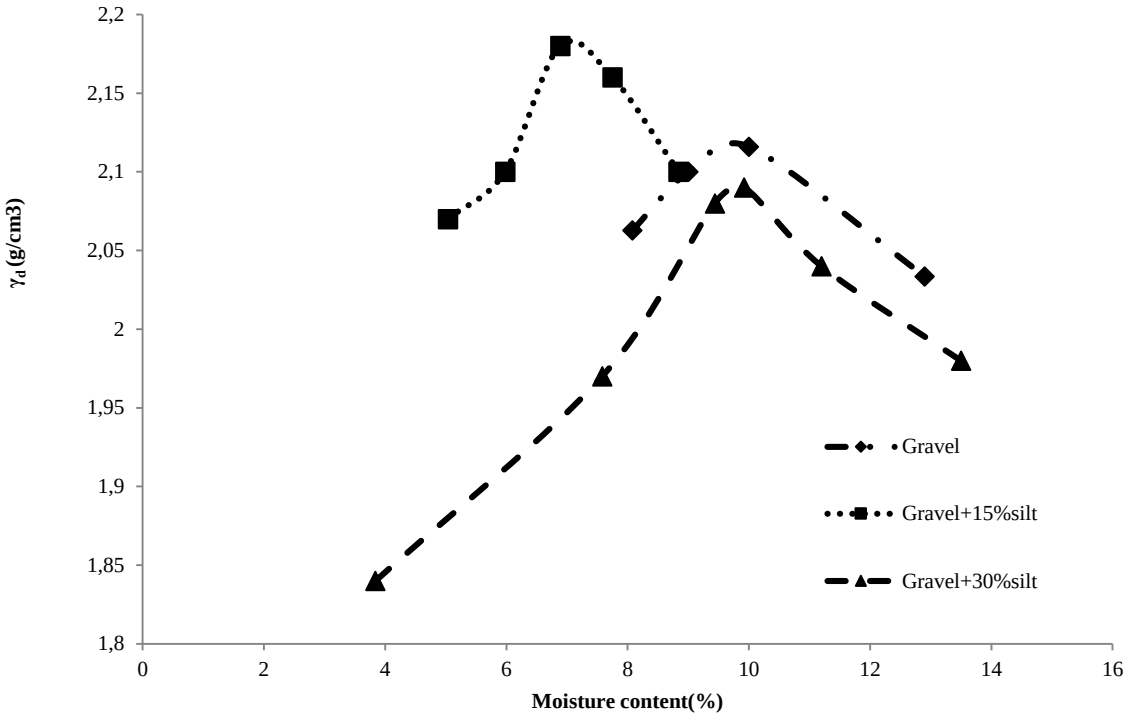

Figure 3. Dry weights values versus moisture content for soils used in this study (Sadeghi azar et al., 2010)

As mentioned above, tests were performed in three relative densities of 90, 95, and 100 percent and the effect of geotextile layer was studied in two position. In the first state, one geotextile layer was placed in the middle of the soil sample, and in the second position two geotextile layers were placed alternatively at equal distances in the sample soil. These position are observed in Figure 4. (Sadeghi azar et al., 2010)

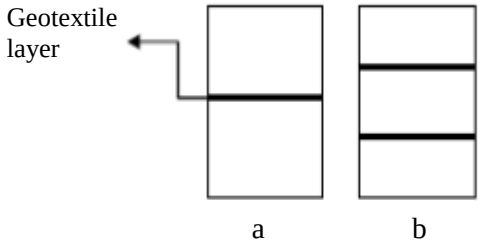

Figure 4. Geotextile positions in this study: a- one layer, b- two layers (Sadeghi azar et al., 2010)

CBR TESTS RESULTS

The results of CBR tests on reinforced and unreinforced soil specimens with different no plastic fines contents are presented below:

1) The amount of the force needed for the piston to penetrate into the specimens was studied without geotextile layers are shown in Figure 5. The results of tests indicated that the bearing capacity of specimens with different compounds increases with an increase in the relative density of the soil. Moreover, with an increase in the amount of non-plastic fines contents in the gravel, the bearing capacity decrease in general.
2) In continue, with placing a geotextile layer in the middle part of the materials, and two geotextile layers at a distance of one third in the sample soils under study. The results of tests are shown in Figures 6, 7, and 8.

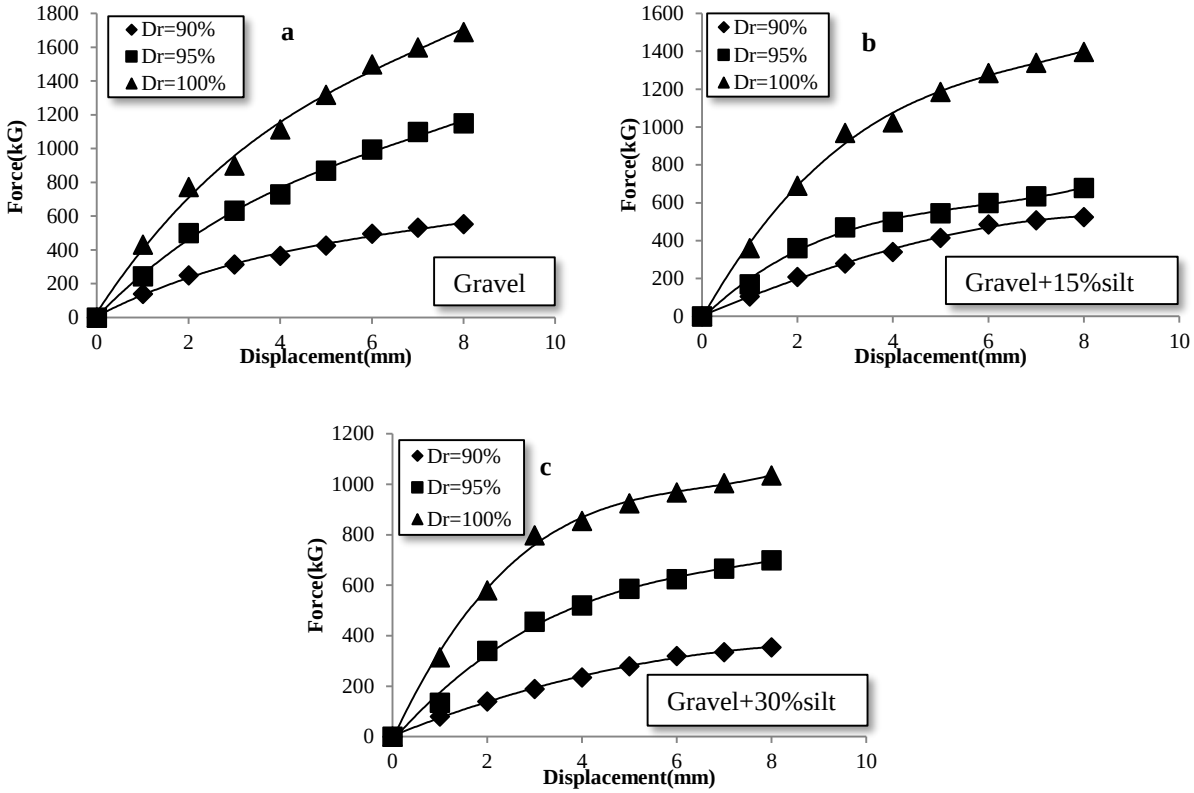

Figure 5. Effects of fines contents on bearing capacity of specimens without geotextile layer in several relative densities (Sadeghi azar et al., 2010)

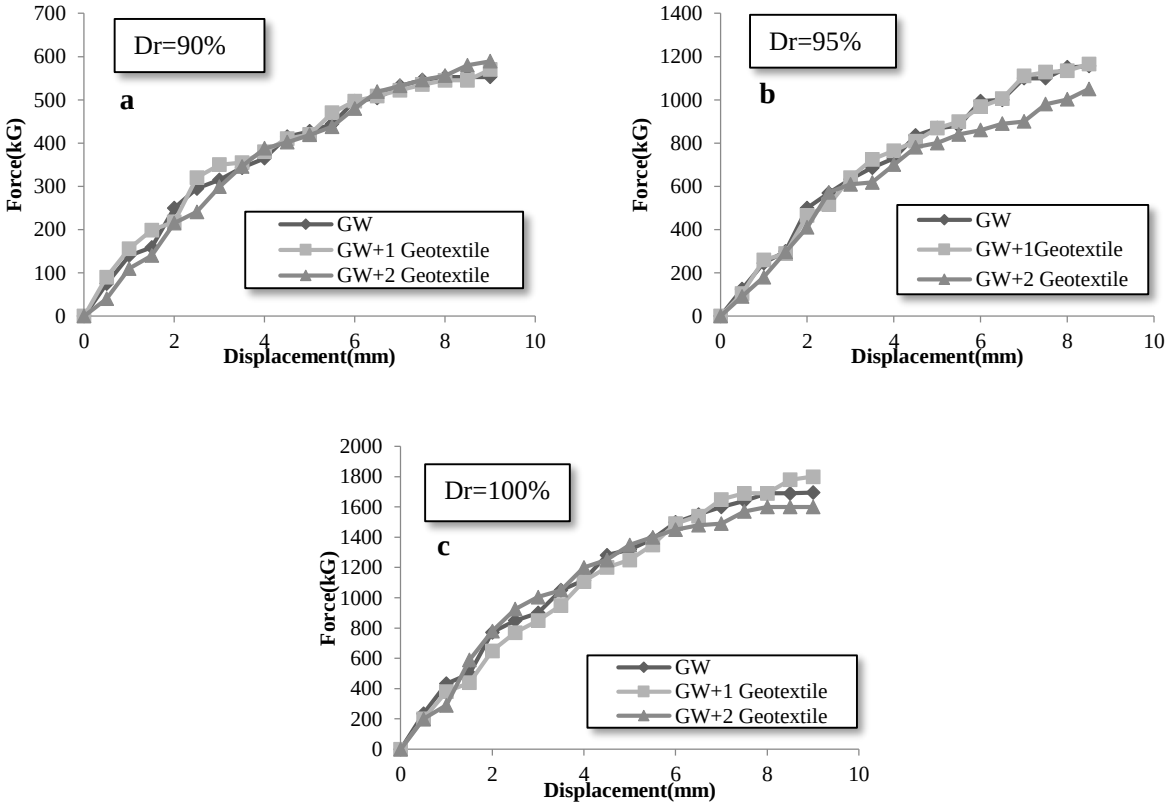

Figure 6. Comparison of gravel bearing capacity in reinforced and unreinforced position in several relative densities (Sadeghi azar et al., 2010)

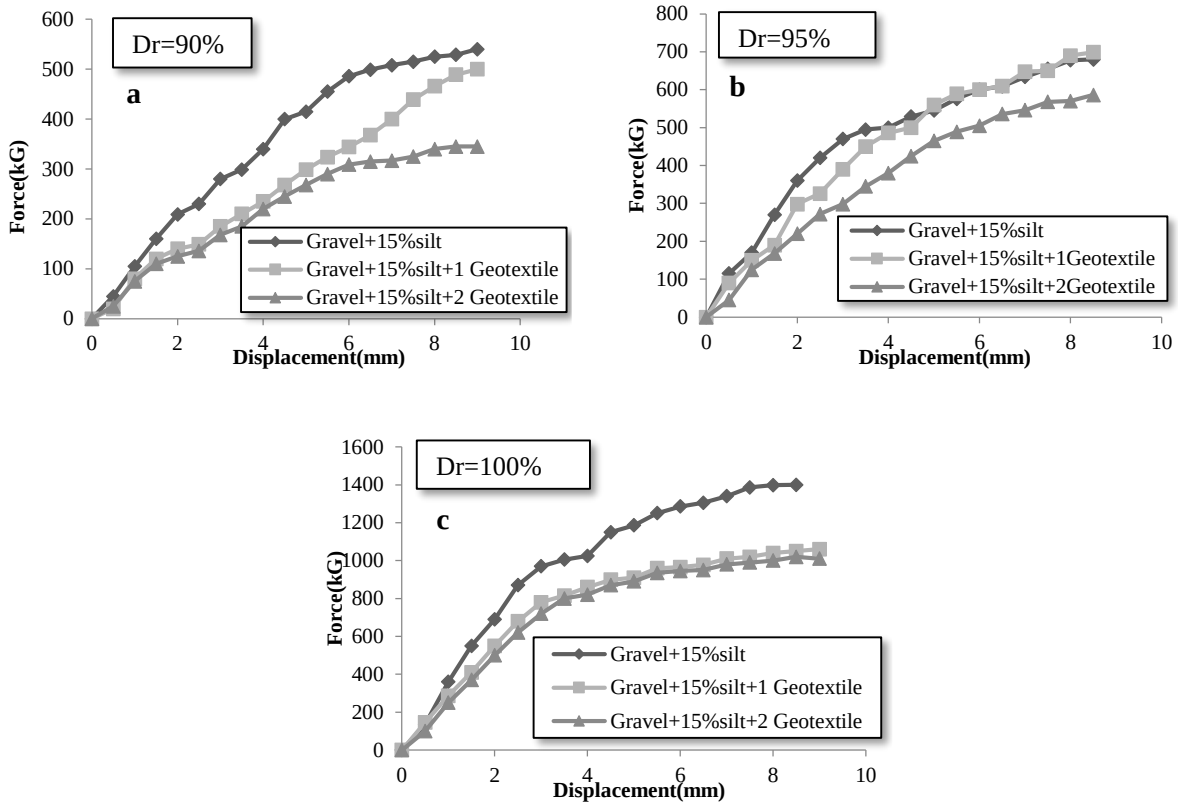

Figure 7. Comparison of gravel+15%silt bearing capacity in reinforced and unreinforced position in several relative densities (Sadeghi azar et al., 2010)

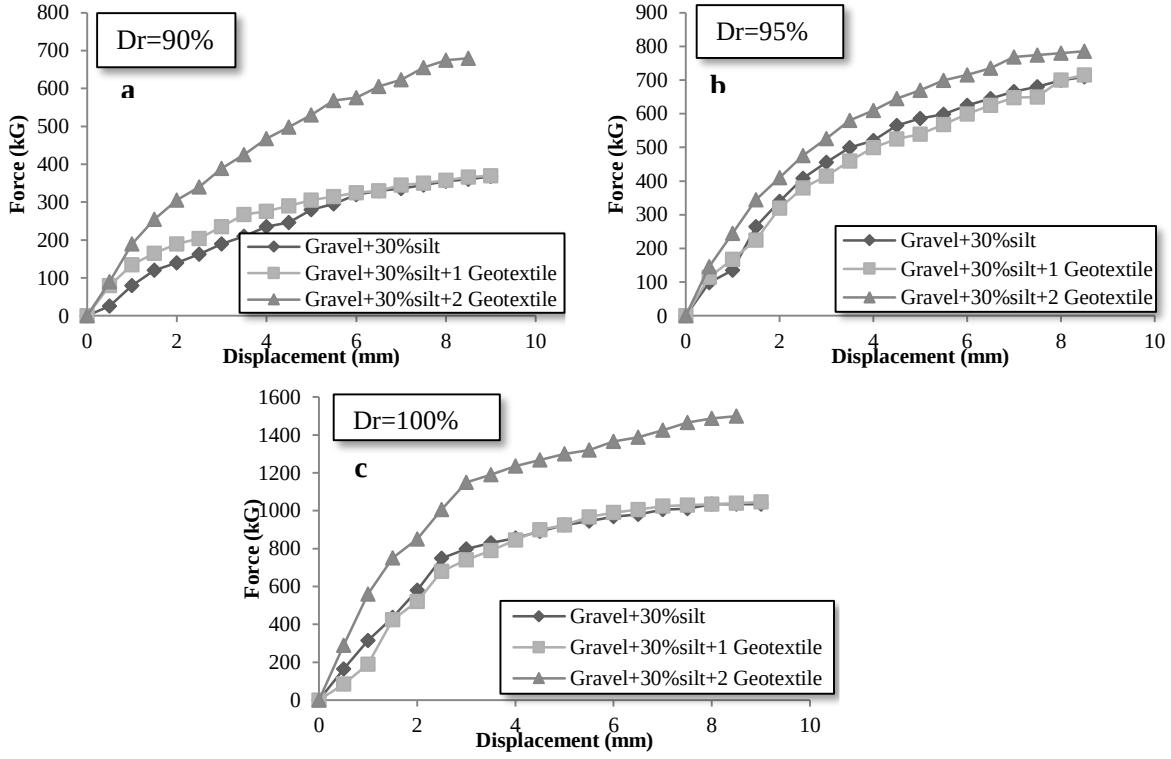

Figure 8. Comparison of gravel+30%silt bearing capacity in reinforced and unreinforced position in several relative densities (Sadeghi et al., 2010)

The Figures are given above indicate that:

a. With an increase in the relative density of the reinforced and unreinforced specimens, the amount of the force needed for the piston to penetrate increases.

b. With an increase of 15 and 30 percent of non-plastic fine contents in the gravely soils, the bearing capacity of the soil decreases gradually.

c. In gravely specimens, at equal relative densities, the bearing capacity of specimen a little increases. But, with placing two geotextile layers resistance decrease.

d. In the gravel+15% silt mixture, at equal relative densities, it is observed that by placing one and two geotextile layers, the bearing capacity of the soil decreases alternatively.

e. In the gravel+30%silt mixture, at equal relative density, it is observed that by placing one and two geotextile layers, the bearing capacity increases, indicating that the bearing capacity of the soil has improved.

f. Generally, with comparing the results, it can understand that at equal relative densities, by placing one and two geotextile layers in the soil specimens, the bearing capacity of the soil increases in comparison with the state in which geotextile layer is not inserted.

3) California Bearing Ratio (CBR) has been evaluated based on ASTM D1883 for the soil specimens and results are observed in Figures 9 and 10. Figure 9 indicates that California Bearing Ratio (CBR) decreases with an increase in the percentage of non-plastic fines content in the gravel. This trend is observed in all relative densities.

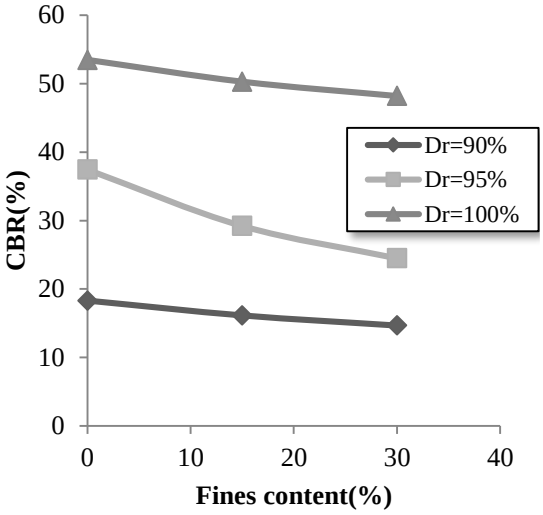

Figure 9. CBR values for various fines content in unreinforced specimen (Sadeghi et al., 2010)

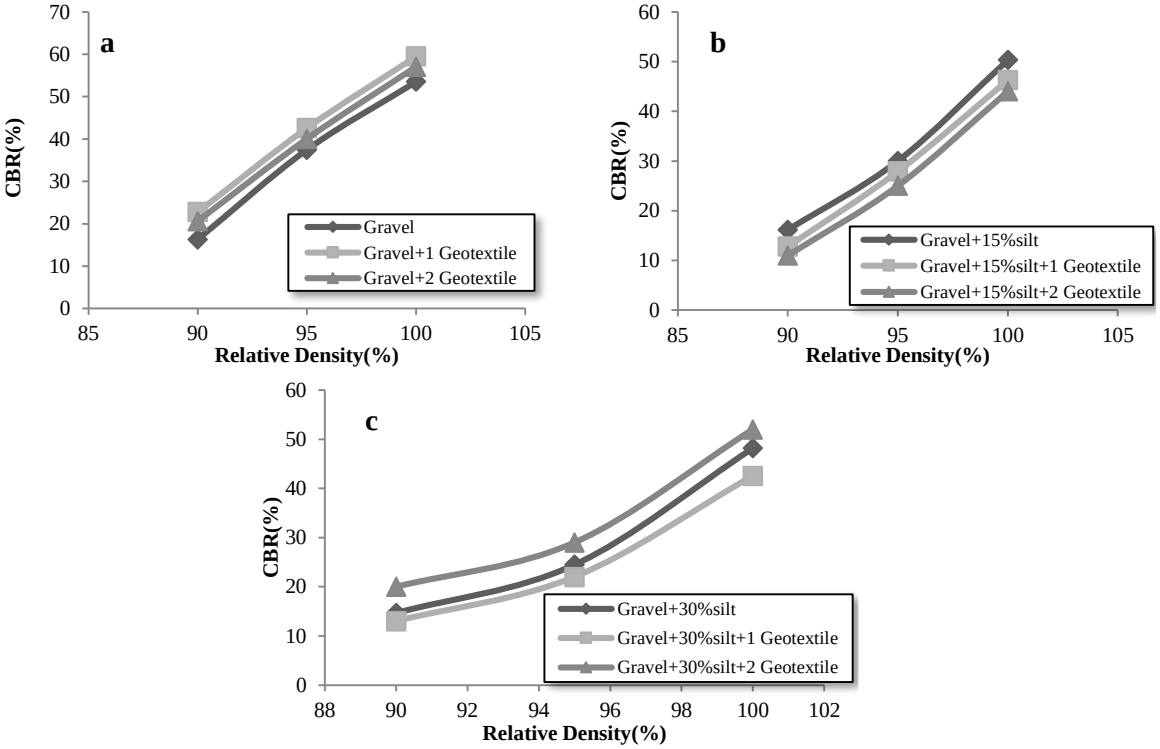

Figure 10. Effects of geotextile layers number on CBR values in specimens (Sadeghi et al., 2010)

Figure 10a show that, the value of CBR in gravelly soil increases with placing a geotextile layer. In continue, by placing two geotextile layers, California Bearing Ratio (CBR) decreases. As can be observed in Figure 10b, in gravel+15%silt mixtures, CBR decreases with placement one and two geotextile layers in specimens of soil continuously. Although, in gravel+30%silt specimens by inserting one geotextile layer the value of CBR decreases a little. But by putting two geotextile layers it increases (Figure 10c).

CONCLUSION AND DISCUSSION

The use of geotextiles in many engineering applications is an effective method in soil improvement. The Review of previous studies show that geotextiles increase bearing capacity in subgrade layer with fines content by being placed between the sub base layers and subgrade. The main purpose of the present study was the experimental study of the effect of the number of geotextile layers on the bearing capacity of the gravel with containing 15 and 30 percent of silt by using California Bearing Ratio (CBR) test. Generally, by observing the results it can be expressed that the resistance and bearing capacity of the gravelly soils containing silt depend on the ratio of gravel and silt mixture. When the percentage of the fine contents is low, and their only role is fillers between the granular particles, the existence of fine particles would not affect resistance greatly; however, if the dispersion of the fine particles is in a way that some of them work as separators between the granular particles, a rather unstable skeleton would be formed in comparison with the original skeleton of the gravel resistance and bearing capacity would decrease. With an increase in the percent of fine particles and when the granular particles are completely separated from each other, the effect of granular particles on bearing capacity of mixture can be disregarded. In this state, resistance is provided just only the fine particles. Therefore, with placement a geotextile layer in the mixture soils, the soils' improvement and increase in bearing capacity can happen. The reason is the fact that by placing one geotextile layer, the natural structure of the specimens do not change dramatically, and particles discontinuity do not happen in them. This increases the bearing capacity of the gravel and increases the resistance of the gravel with 30% of silt. However, it is recommended that further studies can be conducted on the number of geotextile layers and their arrangement in different soil compounds and specimens.

REFERENCES

1. YODER E. J., WITCZAK M. W. Principles of Pavement Design, Second Ed., Wiley Interscience, Newyork, 300-321, 1975.
2. RESL, S., WERNER, G., The influence of nonwoven needle- punched geotextiles on the ultimate bearing capacity of the subgrade, *Proceedings of the Third International Conference on Geotextiles*, Vol. 4, pp. 1009–1013, 1986, Vienna,
3. FANNIN, R.J., O. SIGURDSSON, Field observations on stabilization of unpaved roads with geosyntheticS, *ASCE Journal of Geotechnical Engineering*, 122, 7, 544-553, 1996.
4. BERGADO, D.T., S. YOUWAI, C.N. HAI, P. VOOTTIPRUEX, Interaction of nonwoven needle-punched geotextiles under axisymmetric loading conditions, *Geotextiles and Geomembranes*, 19, 299-328, 2001.
5. RAYMOND, G., ISMAIL, I., The effect of geogrid reinforcement on unbound aggregates, *Geotextiles and Geomembrane*s, 21, 355-380, 2003.
6. PARK, T. and TAN S.A., Enhanced performance of reinforced soil walls by the inclusion of short fiber, *Geotextiles and Geomembranes*, 23, 348–361, 2005.
7. YETIMOGLU, T., SALBAS, O., A study on shear strength of sands reinforced with randomly distributed discrete fibers, *Geotextiles and Geomembranes*, 21,2, 103-110, 2003.
8. PATRA, C.R., DAS, B.M. and ATALAR C., Bearing capacity of embedded strip foundation on geogrid-reinforced sand, *Geotextiles and Geomembranes*, 23, 5, 454-462, 2005.
9. VARUSO, R.J., GRIESNABER, J.B.and NATARAJ, M.S., Geosynthetic reinforced levee test section on soft normally consolidated clays, *Geotextiles and Geomembranes*, 23, 4, 362-383, 2005.
10. HAERI, S.M., NOURZAD R. and Oskrouch A.M., Effect of geotextile reinforcement on the mechanical behavior of sands, *Geotextiles and Geomembranes*, 18, 6, 385-402, 2000.
11. ZHANG, M.X., JAVADI, A.A. and MIN X., Triaxial tests of sand reinforced with 3D inclusions, *Geotextiles and Geomembranes*, 24, 201-209, 2006.
12. LATHA, G.M. and MURTHY V. S., Effects of reinforcement form on the behavior of geosynthetic reinforced sand, *Geotextiles and Geomembranes*, 25, 23-32, 2007.
13. WILLIAMS, E.D. and OKINE, N. A., Effect of geogrid in granular base strength – An experimental investigation, *Construction and Building Materials*, 22, 2180-2184, 2008.
14. NAEINIE S. A. and MIRZAKHANLARI M., The effect of geotextile and grading on the bearing ratio of granular soils, *electronic journal of geotechnical engineering (EJGE)*, 13, 1-10, 2008.

15. NAEINIE S. A. and ZIAIE MOAYED R., Effect of plasticity index and reinforcement on the CBR value of soft clay, *International Journal of Civil Engineering*, 7, 2, 124-130, 2009.

16. SENTHIL KUMAR P. and RAJKUMAR R., Effect of geotextile on CBR strength of unpaved road with soft subgrade, *electronic journal of geotechnical engineering (EJGE)*, 17, 1355- 1363, 2012.

17. GOHARI M., DABIRI R. and RAZIZADEH F., Evaluation of geotextile effects on bearing capacity of granular soils based on California bearing ratio (CBR) test, MSC thesis of Engineering geology, Islamic Azad University, Ahar Branch, 2010. (In Persian)

18. ASTMC25-99, Standard Test Methods for Chemical Analysis of Limestone, Quicklime, and Hydrated Lime, Annual book of ASTM standards, 1999.

19. ASTM D421-85, Dry Preparation of Soil Samples for Particle-Size Analysis and Determination of Soil Constants, Annual book of ASTM standards, 1985(reapproved 1998).

20. ASTM D422-63, Standard Test Method for article-Size Analysis of Soils, Annual book of ASTM standards 1963(reapproved 1998).

21. SADEGHI AZAR K., DABIRI R. and RAZIZADEH F., Study of geotextile layers effects in bearing capacity of granular soils with non-plastic fines content based on California bearing ratio (CBR) test, MSC thesis of Engineering geology, Islamic Azad University, Ahar Branch, 2010. (In Persian)

22. www.earthgoogle.com, Imagery ©2016 Digital Globe, Cnes/Spot Image, CNES / Astrium, Map data ©2016 Google

23. ASTM D 4318-95a, Standard test method for liquid limit, plastic limit an plasticity index for soils, Annual book of ASTM standards, 1995

24. ASTM D1883-93, Standard test method for CBR (California bearing ratio) of laboratory- compacted soils, Annual book of ASTM standards, 1993.

25. ASTM-D 698-00, Standard Test Methods for Laboratory Compaction Characteristics of Soil Using Standard Effort (12,400 ft-lbf/ft^3 (600 kN-m/m^3)), Annual book of ASTM standards, 2000.